Heliyon 10 (2024) e38176

Contents lists available at ScienceDirect

Heliyon

journal homepage: www.cell.com/heliyon

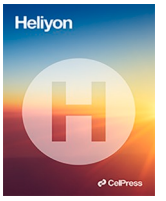

Research article

Geochemical exploration for tantalum in coltan-rich pegmatites at Bewadze-Mankoadze area of the Kibi-Winneba Belt, southern Ghana: Constraints from exploratory data analysis

Emmanuel Daanoba Sunkari [a,b,*], Joshua Nkansah [a], Salaam Jansbaka Adams [c,d]

[a] Department of Geological Engineering, Faculty of Geosciences and Environmental Studies, University of Mines and Technology, P.O. Box 237, Tarkwa, Ghana
[b] Department of Chemical Sciences, Faculty of Science, University of Johannesburg, P.O. Box 524, Auckland Park 2006, Johannesburg, South Africa
[c] School of Natural and Environmental Sciences, University of Environment and Sustainable Development, PMB –Somanya, Eastern Region, Ghana
[d] School of Nuclear and Allied Sciences, College of Basic and Applied Sciences, University of Ghana, P.O. Box LG 80, Legon – Accra, Ghana

ARTICLE INFO

Keywords:
Tantalum
Pegmatites
Multivariate statistical analysis
Geochemical anomalies
Pathfinder elements

ABSTRACT

The Bewadze-Mankoadze pegmatites in the Kibi-Winneba Belt of Ghana host several columbite group minerals (WGM) and wodginite group minerals (WGM) as well as other rare and radioactive elements such as uraninite and cesium. In this study, petrographic studies of rock samples from pegmatite outcrops and statistical analysis of the major and minor elements were conducted to identify the pathfinder elements of a new tantalum deposit in the area. Ten samples were obtained from each town for whole-rock geochemistry and thin sections were prepared from some of the samples taken for petrographic analysis. The petrographic analyses showed the presence of quartz, K-feldspars, plagioclase, muscovite, spodumene, albite, tourmaline, columbite group minerals, and montebrasite, which indicate that the studied samples are granitic pegmatites. The geochemical data of the 10 samples obtained from each town showed high concentrations of Cr, Cs, Rb, Sm, and Ta. The Ta concentrations ranged from 10.5 to 773 ppm with an average value of 260 ppm. Q-Q plots showed outliers and variations from the dataset's normal distribution, which were fixed by centred log-ratio transformation and demonstrated to be normal by the Kolmogorov-Smirnov test and Shapiro-Wilk test for normality. Spearman correlation revealed that Sc, Ga, Nb, and Cs showed a moderate to strong correlation with Ta. Factor analysis indicated elemental association of Ta with Cs, Zn, Nb, MgO, Sc, Ga, and V. Three (3) multi-element relationships were discovered by hierarchical cluster analysis: (1) As, La, Hf, CaO, U, Co, Pb, Ce, Ba and Na_2O, (2) V, Nb, Ta, Ga, Sc, Cr, Cu, Nb and MgO, and (3) Ni, SiO_2, Cs, Zn, Sm, Rb, K_2O, Y, Th, Al_2O_3 and Fe_2O_3. Hence, a comparison of the results of the multivariate statistics established Sc, Ga, Nb, and Cs as the pathfinders of tantalum in the Bewadze-Mankoadze area. Geochemical anomalies involving these elements can be observed in the south-western portion of the study area, according to single and multi-element halo mapping. It is therefore recommended that exploration activities for tantalum mineralization should focus on the south-western part of the study area, where the anomalies of the pathfinder elements are located.

* Corresponding author. Department of Geological Engineering, Faculty of Geosciences and Environmental Studies, University of Mines and Technology, P.O. Box 237, Tarkwa, Ghana.
E-mail address: edsunkari@umat.edu.gh (E.D. Sunkari).

https://doi.org/10.1016/j.heliyon.2024.e38176
Received 3 June 2024; Received in revised form 18 September 2024; Accepted 19 September 2024
Available online 21 September 2024

1. Introduction

Tantalum (Ta) and other critical elements such as Be, Cs, Li, Nb, Sn, U and Th drive their economic sources from pegmatites. The study of pegmatites has therefore attracted a lot of attention in recent years because these elements they contain are critical towards clean energy transition [1–7]. Pegmatites are texturally and compositionally complex igneous rocks exhibiting skeletal, radial, and graphic crystal intergrowth patterns, as well as strong anisotropy of crystal orientations from the edges inward, mineralogical zonation, and coarse but variable crystal size. However, most pegmatite deposits are made of simple mineralogy such as quartz, feldspar and mica, and have a silicic composition identical to granite [8].

Pegmatites containing rare elements can be grouped into three types which are: Lithium–Cesium–Tantalum (LCT) pegmatites, which have high concentrations of Li, Cs, Ta, B, Be, P, F, Ga, Mn, Sn, Nb, Rb, and Hf [9–11]. The Winneba-Mankoadze pegmatites in Ghana [1,3,5–7] as well as the Greenbushes, Wodgina, and Pilgangoora pegmatites in Western Australia, the Tin Mountain pegmatite in the United States, Altai Number 3 pegmatite in China, Tanco pegmatite in Canada, Kenticha pegmatite district in Ethiopia, and Bikita pegmatite in Zimbabwe are all examples of major LCT pegmatite deposits [12,13]. The second kind is Niobium-Yttrium-Fluorine (NYF) pegmatites, which exhibit enrichment in B, Be, Sn, Nb > Ta, Y, Ti, REEs, Th, Zr, Sc, U, and F but depleted in Rb, Cs, and Li [9–11]. As summarised by Ref. [9], the Stockholm granite, Ytterby pegmatite group, Grotingen granite, Abborselet, and other related pegmatites in Sweden; the South Platte granite and pegmatite system in Colorado; and the Lac du Bonnet biotite granite and Shatford Lake pegmatite group in Canada, are good examples of NYF pegmatite deposits. It is postulated that contamination of NYF pegmatites during the magmatic or post-magmatic stage is what formed the third type, known as mixed or "hybrid" rare-element pegmatites, which have blended rare-element signatures [9–11,14]. For instance, they might form when freshly crystallised NYF pegmatites are re-melted by metasomatic fluids that are enriched in Li, B, Ca, and Mg. Mixed pegmatites can be found, for instance, in Kimito in Finland, the O'Grady batholith in Canada [14], and the Tordal area of Norway [2].

[6,7] concluded that the pegmatites in the Bewadze-Mankoadze area of the Kibi-Winneba Belt are of the rare element class, LCT (Li-Cs-Ta) subclass, hosted by columbite-tantalite. From this knowledge, this research seeks to focus on the metal tantalum (Ta) hosted in the pegmatites due to its significant concentrations.

Pegmatites are the host of the majority of the economic deposits of tantalum globally. Tantalum has the chemical symbol Ta and the atomic number 73. Tantalus, a figure from Greek mythology, inspired the term tantalium [15]. Tantalum is a shiny, ductile, blue-gray transition metal with extraordinary hardness. It is a refractory metal that is frequently added to powerful alloys with high melting

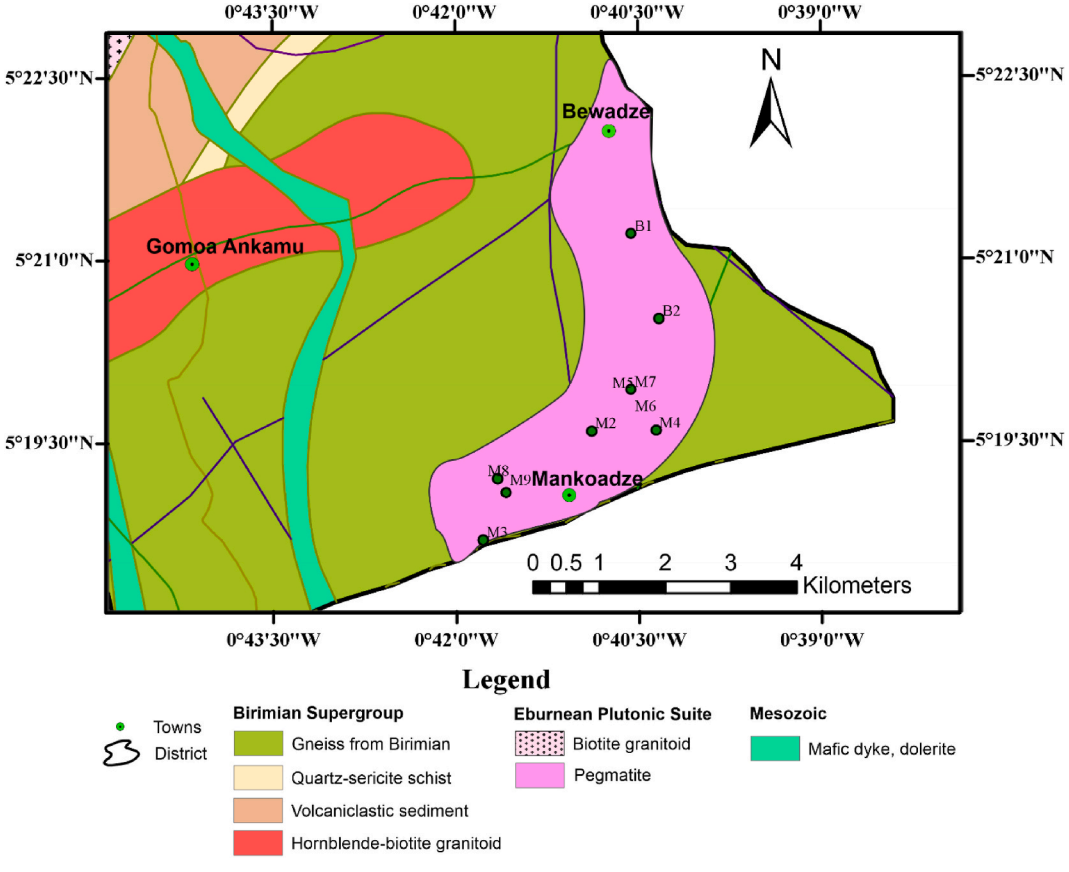

Fig. 1. Geological map of the Gomoa West District showing the Bewadze-Mankoadze towns.

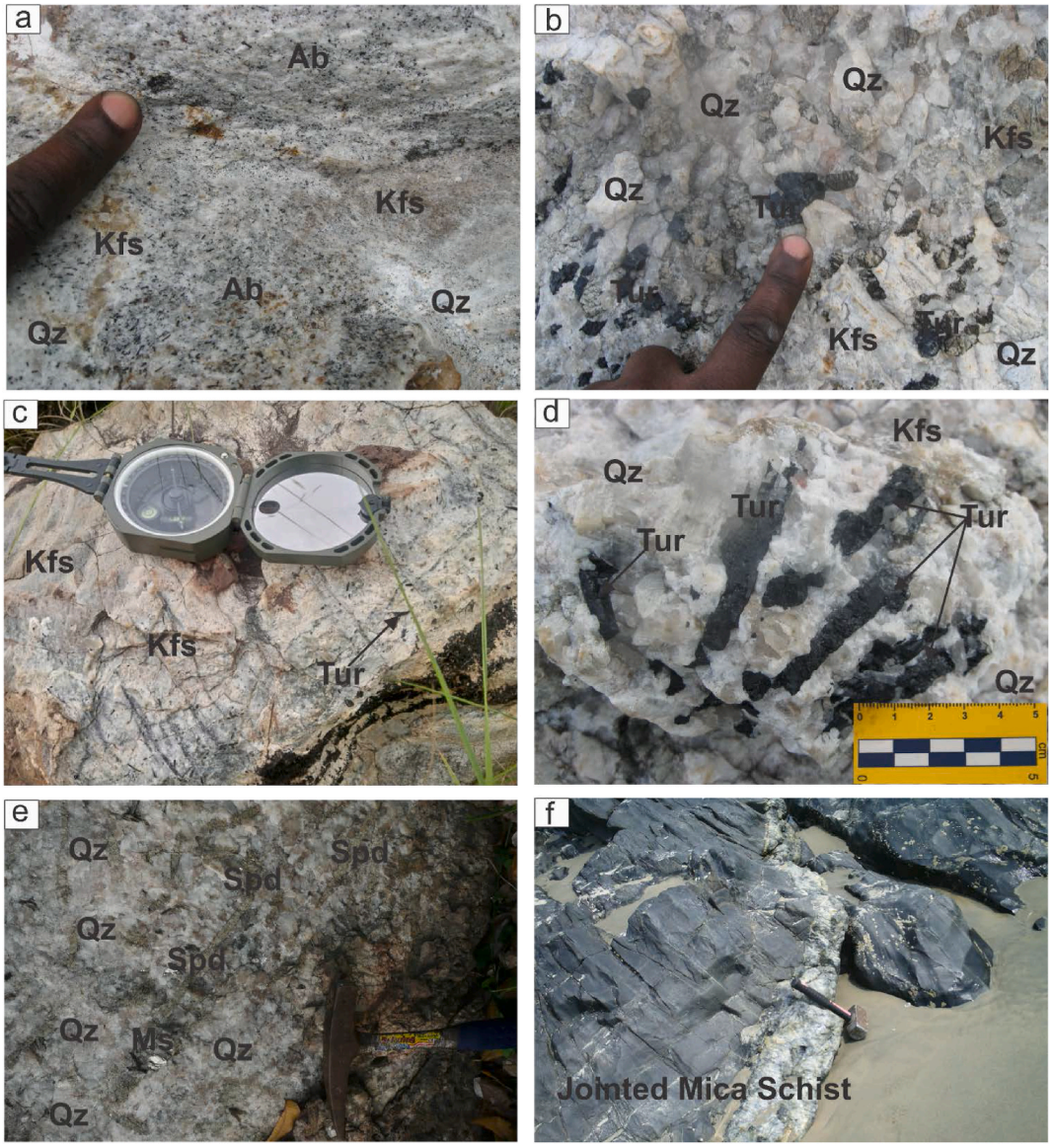

Fig. 2. Field photographs of pegmatites in Bewadze-Mankoadze area (Qz = Quartz, Kfs = Potassium Feldspar, Ab = Albite, Ms = Muscovite, Tur = Tourmaline, Spd = Spodumene).

points. Tantalum is a group 5 element that is always found in geologic sources next to the chemically related element, niobium [15]. Tantalum is a critical metal in today's advanced technological applications. The extraction process takes place from oxide minerals that are present as trace amounts in granitic rare-element pegmatites and rare-metal granites (REP). Exploitation of Nb-Zr-rare earth element (REE) from carbonatites and peralkaline igneous rocks is a promising by-product of mining spodumene from pegmatites. Most of the current Ta production comes from columbite-group minerals (CGM), with minor contributions from ixiolite, rutile, tapiolite, wodginite and pyrochlore-supergroup minerals [16]. Africa's estimated Ta resources are greater than 50,000 tons of contained Ta_2O_5, accounting for 16 % of global resources [16].

Previous studies have reported the presence of rare earth metals in the pegmatites in the Bewadze-Mankoadze area of the Kibi-Winneba volcanic belt [1,3,6,7] but the geochemical characteristics and exploration implications for the mineral tantalum in the pegmatites have not been well documented [6,7]. investigated the mineralogical and petrogenetic features of the pegmatites and concluded that the pegmatites are highly fractionated resulting in the enrichment of light rare earth elements (LREE) than middle rare earth elements (MREE) and heavy rare earth elements (HREE). The authors further indicated that the pegmatites formed in late to post orogenic tectonic settings with calc-alkaline affinities. With that, this research seeks to investigate the exploration implications for tantalum mineralization in pegmatites at Bewadze-Mankoadze area within the Kibi-Winneba metavolcanic belt in the southern part of Ghana. It will help identify the geochemical vectors of the mineral tantalum as a new mineral deposit to mining companies seeking to

expand their operations and increase their output.

2. Geology of the area

The pegmatites at the Bewadze-Mankoadze area which is located along the coast of Ghana forms part of the Birimian Supergroup (2195-2072 Ma) [17], which lies at the southernmost end of the West African Craton [1,3,6,7]. Ghana's Paleoproterozoic Birimian Supergroup is made up of six metavolcanic ("greenstone") belts, five of which are parallel, regularly spaced and exhibit northeast-trending. The easternmost of these belts, the Kibi-Winneba metavolcanic belt, is where the Bewadze-Mankoadze area is located [17,18]. According to Ref. [17], the ''greenstones'' (mainly quartz-hornblende-actinolite schist), amphibolite, and hornblende-biotite-quartz schist are the host rocks of the Bewadze-Mankoadze area (Fig. 1). These rocks have hornblende- and biotite-bearing intrusions. Magnesite and ultramafic tectonic dykes are often intruded into the rocks along foliation planes that follow the NE-SW Birimian trend. Granitoids with accompanying pegmatite and quartz veins run NE and abruptly dip between 70 and 84° to the SE [17,18]. The dykes, which are typically 30 m wide, have undergone partial or complete amphibolite (hornblendite) transformation. Meta-basalts along the shore west of Mankoadze provide evidence of late-stage volcanic activity [17]. The Kibi-Winneba volcanic belt, on the other hand, stretches from Winneba in the Central Region along the coast and strikes northeast for about 100 km into Kibi in the Eastern Region and beyond. The Cape Coast granitoid divides it into northern and southern halves, and it has a basic synclinal structure with the Ashanti and Bui belts [19,20]. The sites of the widespread quartz-veined pegmatites and aplites that are found across the belt are frequently closer to the large extent contacts with the basin-type granitoids. Most of the sills and dykes in this area of the belt appear to be north-south (N-S) trending and have experienced early-stage metamorphism. A few dolerite dykes do not appear to have undergone metamorphism [21].

The Paleoproterozoic Birimian Supergroup (2195-2072 Ma) of Ghana was intruded by syn-volcanic granitoids during the Eburnean orogeny (2120-2115 Ma). The last stage of this Eburnean tectonism is pegmatitic veining [17]. However, the exact age of the Birimian pegmatites is unknown but they are believed to be of post-Eburnean age.

3. Materials and methods

3.1. Field mapping and sample collection

Fresh pegmatite samples from the Bewadze and Mankoadze communities were collected for this study. Ten samples were taken from each study area and labelled accordingly, B and M for samples taken from Bewadze and Mankoadze, respectively. The surface of the in-situ pegmatites was broken off to obtain fresh samples since those on the surface were altered. This was done to collect fresh samples for good petrographic studies. Field photos of the pegmatite exposures are shown in Fig. 2.

3.2. Petrographic and bulk-rock geochemical analyses

Eight pegmatite samples were selected for thin section preparation and analysis. To identify the minerals and their relationships, thin sections of pegmatites from the Bewadze-Mankoadze area were examined with a transmitted-light microscope, LEICA DM2700P housed at the Geological Engineering Department of the University of Mines and Technology, Ghana. Various optical characteristics, including colour, texture, twining, pleochroism, extinction angle, cleavage, bireflectance, and isotropism/anisotropy were used to discriminate between different minerals.

In this study, 50 samples were collected from Bewadze-Mankoadze area for whole-rock geochemical analysis. The samples were prepared for the geochemical analysis at the Ghana Research Reactor-1 (GHARR-1) laboratories. The geochemical analysis was carried out by Ref. [7] using standard methods including X-ray Fluorescence Spectroscopy (XRF) at the Ghana Geological Survey Authority, Accra, and Instrumental Neutron Activation Analysis (INAA) at the Ghana Atomic Energy Commission, Kwabenya - Accra.

3.3. Data synthesis and statistical analysis

3.3.1. Q-Q plots

The quantiles of a dataset are compared to the quantiles of a selected theoretical distribution using a Q-Q plot. The standard normal distribution is the theoretical distribution that is most frequently utilised. The link between the observed quantiles and the corresponding quantiles anticipated under the distribution is shown in the Q-Q plot. Q-Q plots are widely used to evaluate a dataset's assumed normality [22,23]. If the observed data points closely resemble a normal distribution, the diagonal line may be a good approximation for the data [24].

3.3.2. Kolmogorov smirnov and Shapiro Wilk tests

It is frequently important in statistical analysis to compare two datasets or determine whether a dataset fits a specific distribution. With the use of the robust statistical test known as the Kolmogorov-Smirnov, the ability of a single dataset to comply with a certain theoretical distribution or whether two datasets exhibit the same distribution can be assessed [25]. The supremum class of EDF (Empirical Distribution Function) statistics, which includes the Kolmogorov-Smirnov statistic (referred to as KS), is based on the greatest vertical variation between the predicted and observed distribution [26]. For n ordered data points $x_1 < x_2 < \ldots < x_n$, the test statistic according to Conover [26] can be computed from equation 1.

$$T = \sup_x |F^*(x) - F_n(x)| \quad (1)$$

where;

sup = stands for supremum which means the greatest.

$F^*(x)$ = the hypothesized distribution function

$F_n(x)$ = the EDF estimated based on the random sample

In KS test of normality, $F^*(x)$ is a normal distribution with known mean, μ, and a standard deviation, σ.

The KS test statistic is meant for testing,

H0: $F(x) = F^*(x)$ for all x from -∞ to ∞ (the data follows a specified distribution)

Ha: $F(x) \neq F^*(x)$ for at least one value of x (the data do not follow the specified distribution).

If T is more than the 1-α quantile, H_0 at the level of significance is neglected, α based on the quantile table for the Kolmogorov test statistic. The dataset is said to be normal when it has a significant value greater than or equal to 0.05 ($\alpha \geq 0.05$)

The Shapiro-Wilk test, introduced in 1965 by Samuel Sanford Shapiro and Martin Bradbury Wilk, is a widely used statistical technique for determining if a dataset has a normal distribution. If the p-value is greater than the chosen significant level, typically 0.05, the null hypothesis is accepted; however, if the p-value is less than the significant level, the null hypothesis is rejected, indicating that the dataset deviates significantly from a normal distribution.

3.3.3. Spearman's correlation

According to Ref. [23], the two-tailed Spearman's Correlation approach may be used to identify the link between any two geochemical variables while considering their multivariate and regionalised nature. The degree and direction of the monotonic link between ranking variables are evaluated using the Spearman correlation test, a commonly used statistical technique. The null hypothesis of the Spearman correlation test is the assumption that the variables do not have a monotonic relationship. The test statistic, indicated as rho (ρ), reflects the strength and direction of the correlation, and has a range from −1 to 1. In contrast, a negative rho denotes a negative monotonic connection. A positive rho denotes a positive monotonic relationship [27].

3.3.4. Centred log-ratio (CLR) transformation

Given the deviation of geochemical data from normal distribution, the resulting multi-element dataset's lowest and maximum contents are lessened by the Centred Log Ratio (CLR) Transformation [22,23], which can be calculated from equation (2).

$$CLR(x) = \left(log\left(\frac{x_1}{g(x)}\right), \ldots, log\left(\frac{x_n}{g(x)}\right) \right) \quad (2)$$

where;

x = composition vector

$x_1, x_2, \ldots, x_n$ = single elements in the samples

g(x) = geometric mean.

3.3.5. Factor and hierarchical cluster analyses

Factor analysis (FA), which uses the principal component approach, is a multivariate statistical method that may be used to identify element relationships [23]. According to Ref. [28], the main objective of factor analysis is to uncover hidden multivariate data structures and to reduce the number of "factors" necessary to adequately explain the variation in a multivariate data collection. The Kaiser criterion was applied to determine the number of components to be extracted. Only key components with eigenvalues of 1 or more are extracted using the Kaiser criteria. The covariance matrix and scree plots both display the number of components and the similarity index, respectively [29].

Dendrograms were used to display results of the hierarchical cluster analysis (HCA). The dendrogram displays the steps taken by the program to arrive at the answer, the multi-element clusters, and the distances (referred to as the squared Euclidean distance) separating these multi-element clusters [29]. According to Ref. [29], the HCA technique is described by the computation of the similarity of X number of components. Following that, two components are clustered under the constraint that a given agglomeration criteria will be decreased because of the clustering. The two items are in a class that is created by this clustering. Furthermore, in the aforementioned situation, two elemental classes are brought together by examining the resemblance or discrepancy between the previously constructed class and the N-2 remaining components. This step is continued until all the components have been clustered.

3.3.6. Delineation of geochemical anomalies

Anomaly thresholds were determined to distinguish anomalies from background values; anomalies of interest in geochemistry are those values that exceed the threshold. Calculating threshold anomalies for defining anomalies involves using the median absolute deviation of [30]. The anomaly threshold can be expressed in equation (3) as:

$$T = med + 2MAD \quad (3)$$

where;

T = anomaly threshold

med = median value of the analysed elements.

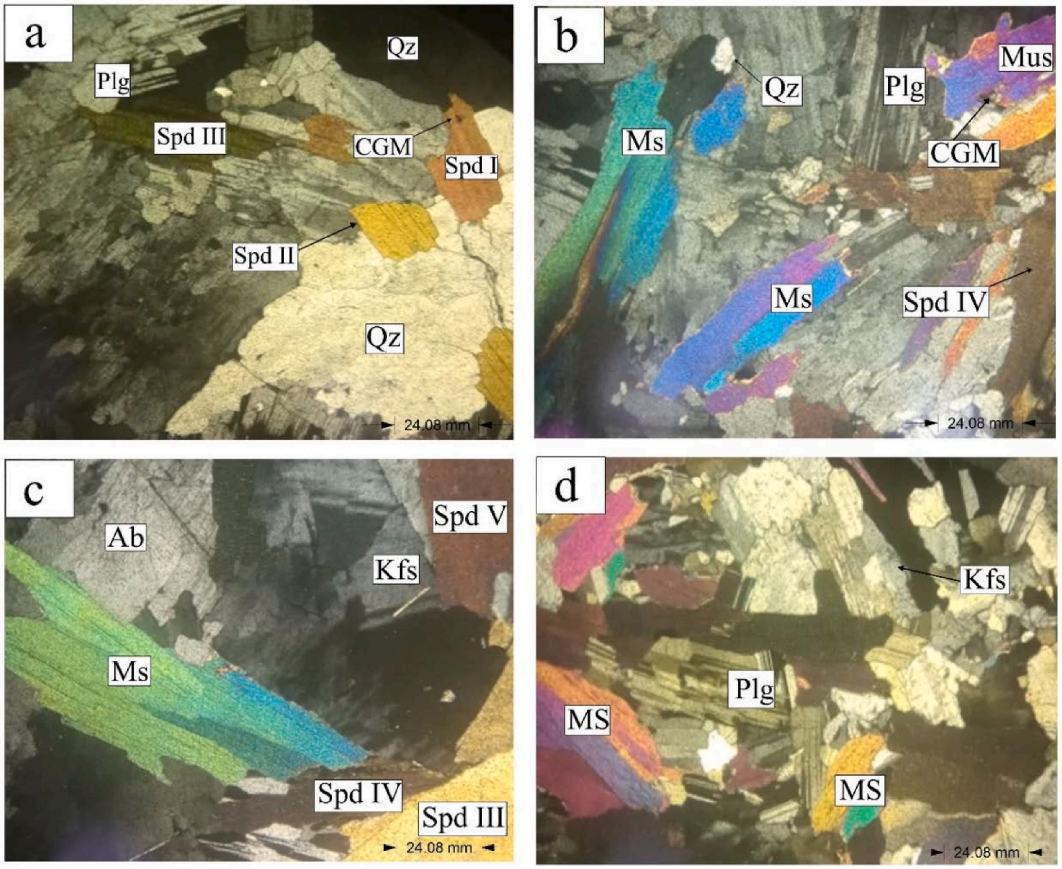

Fig. 3. Photomicrographs of pegmatites in the Bewadze area under transmitted light (Qz = Quartz, Spd = Spodumene, Plg = Plagioclase, Ms = Muscovite, Kfs = Potassium Feldspar, Ab = Albite, CGM = Columbite Group Minerals).

MAD = median absolute deviation.

According to Ref. [30], the MAD (median absolute deviation), which measures data dispersion, is the most accurate statistical indicator of variability in a univariate sample of quantitative data. MAD is determined using the formula (equation (4)):

$$MAD = median\ |xi - median\ (xi)| \tag{4}$$

where xi is the element concentration.

An approach known as the "multi-element halos technique" can be used to outline geochemical halos surrounding mineral deposits more effectively than using only one pathfinder element [31]. This approach allows one to use the formula (equation (5)) to get the threshold values for the multi-element halos:

$$H(X+Y) = \left(\frac{X_1}{X_0} + \frac{Y_1}{Y_0}\right);\ \left(\frac{X_2}{X_0} + \frac{Y_2}{Y_0}\right); \ldots;\ \left(\frac{X_N}{X_0} + \frac{Y_N}{Y_0}\right) \tag{5}$$

where;

X_1, X_2, …, X_N = concentrations of X in samples 1, 2, …, N.

Y_1, Y_2, …, Y_N = concentrations of Y in samples 1, 2, …., N.

X_0 and Y_0 = threshold values of X and Y elements.

The single and multi-element threshold outcomes helped construct the geochemical anomaly maps of the research area using the Inverse Distance Weighting (IDW) Method. Maps of single and multi-element anomaly dispersions were produced with the Geographic Information System application software, ArcMap 10.7.1.

4. Results and discussion

4.1. Field relations and petrography of the Bewadze-Mankoadze pegmatites

Geological field mapping was first conducted to understand the trend of the pegmatites. It was observed that the pegmatites were

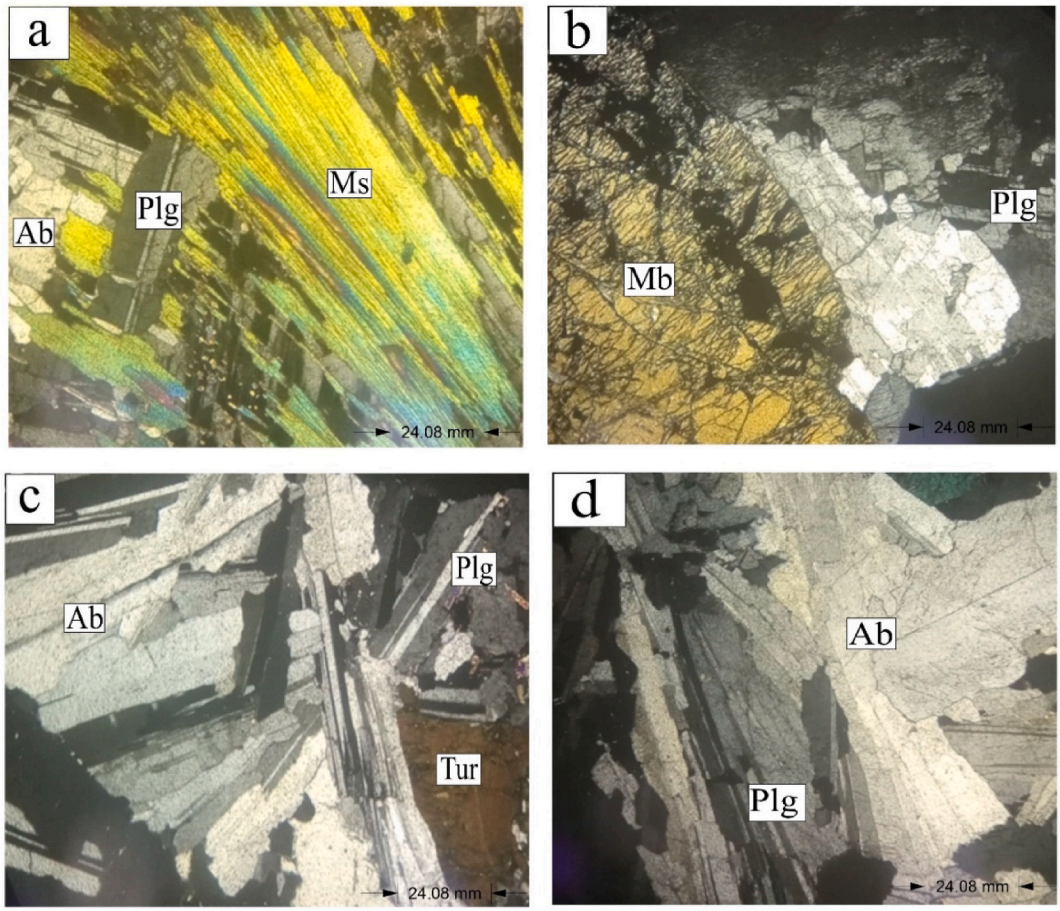

Fig. 4. Photomicrographs of pegmatites in the Mankoadze under transmitted light (Ab = Albite, Plg = plagioclase, Ms = Muscovite, Mb = Montebrasite, Tur = Tourmaline).

trending in the NE/SW direction as shown in the geological map (Fig. 1). Rocks found included gneiss-hosted pegmatites with a few quartz veins running through them, as well as mica schist towards the coast (Fig. 2a–f). They have an average dip reading of 43° and a strike of 064°. The pegmatite outcrops generally occur as smaller oval or tabular outcrops (Fig. 2a–c and e) except north of the Egyasimaku hills where a huge, elongated outcrop occurs (30 m × 10 m) (Fig. 2b and d). They also occur as dykes intruding the mica schists along the coast of Mankoadze (Fig. 2f). Pegmatites occur at Bewadze whiles both pegmatites and aplites occur at Mankoadze. The aplites which contain green beryl and apatite largely occur at the northern and eastern parts of the Egyasimaku hills. The pegmatites are coarse-to very coarse-grained whiles the aplites are fine-to medium-grained. The texture of the mineral grains is similar to the texture of the pegmatites and aplites as reported by Refs. [3,6,7].

In terms of mineralogical composition, quartz, K-feldspar, albite, muscovite, spodumene, and black tourmaline were identified under macroscopic view (Fig. 2a–f) during the field mapping. The tourmaline minerals are medium-grained in the aplites (Fig. 2a and g) and medium-to very coarse-grained in the pegmatites (10 cm × 1 cm) (Fig. 2d). The spodumene are also coarse-grained (5 cm × 1 cm) (Fig. 2e). Other accessory minerals include pinkish garnet, columbite- and wodginite-group minerals [6,7].

Study of the Bewadze-Mankoadze pegmatites under the microscope shows anhedral to subhedral crystals. They are dominated by minerals including quartz, K-feldspars, plagioclase, muscovite, spodumene, albite, tourmaline, columbite group minerals, and montebrasite (Fig. 3a–d; Fig. 4a–d) similar to the pegmatites of the Cape Coast sedimentary Basin of the Birimian Supergroup of Ghana [32], the pegmatites of the Zenaga inlier in the Anti-Atlas, Morocco [33] and the Shigar Valley pegmatites, Pakistan [34]. Quartz in the pegmatites was observed to have a first order of gray. Some other part of the quartz exhibits undulose extinction due the shattering and deformation of the quartz mineral [35]. Potassium feldspar under the microscope had a second order dark-gray interference colour and a distinctive twinning structure. Plagioclase was also observed to be displaying polysynthetic twining that is a zig-zag extinction pattern due to its anisotropic nature. Muscovite and spodumene appeared to be the same but spodumene was more pleochroic than muscovite. Muscovite had colours ranging from green to blue to purple and that of spodumene had differentiated colours due to the presence of varying elements in different spodumene types. The colour variation in spodumene occurs because of different impurities (e.g., Mn or Fe) in the mineral [36]. This resulted in the differentiation of the spodumene into spodumene I, II, III, IV, and V based on the range of alteration colours (Fig. 3a–d; Fig. 4a–d). Also, muscovite had even cleavage plane whilst that of spodumene were uneven.

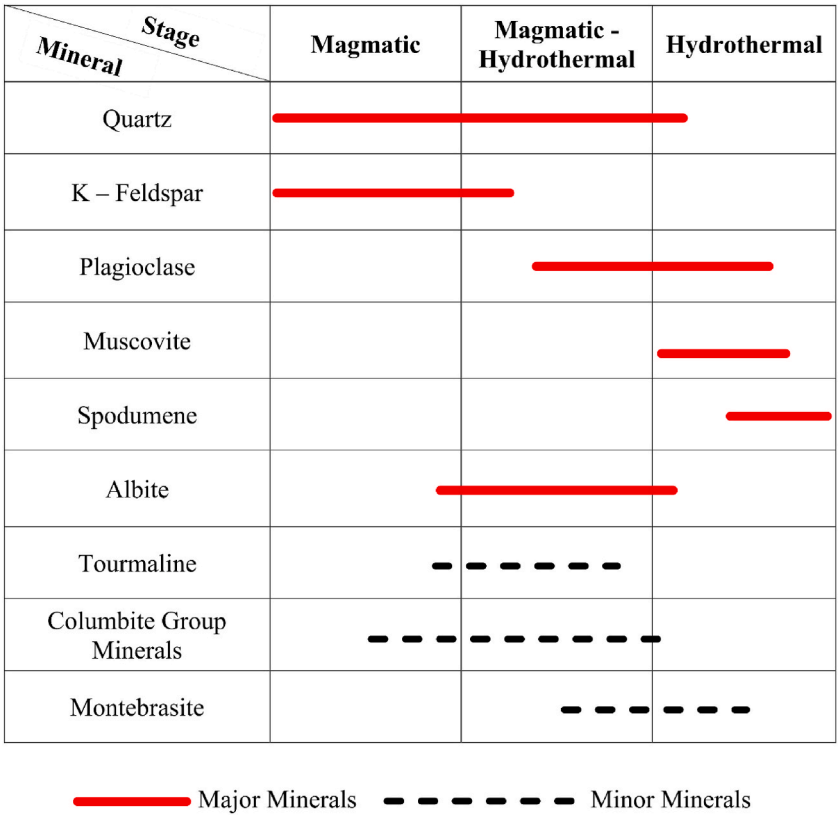

Fig. 5. Paragenetic sequence of mineral formation.

Albite was also seen to be exhibiting perthitic texture under the microscope. Globally, Ta has been reported to occur largely in complex-type pegmatites and albite-rich aplites [4,9,37,38]. Hence, the high values of Ta at the Bewadze-Mankoadze area can be concluded to be because of the occurrence of albite-rich pegmatites-aplites in the area as observed in the thin sections (Fig. 3a–d; Fig. 4a–d). The columbite group of minerals appeared in black spots indicating the high presence of tantalite in them. Splintery fractures were displayed by montebrasite having a first order colour of yellow.

4.2. Mineral assemblage paragenesis

The Ta mineralization and the formation of the host rock occurred in three stages: magmatic, magmatic-hydrothermal and the hydrothermal stage (Fig. 5). During the magmatic stage the host rock began to form, and minerals related to the host rock like quartz started to form in the magmatic stage and run into the magmatic hydrothermal stage and partly in the hydrothermal stage. K-feldspars also started forming in the magmatic stage and ended up partly in the magmatic hydrothermal stage.

Plagioclase began forming in the magmatic-hydrothermal stage and ended up in the middle of the hydrothermal stage. Muscovite also behaved similarly to the K-feldspar, forming in the magmatic stage, and ending up partly in the magmatic-hydrothermal stage. Spodumene also started forming towards the end of the hydrothermal stage. Albite, tourmaline and the columbite group of minerals developed towards the end of the magmatic stage moving into the magmatic-hydrothermal stage. Montebrasite started forming in mid magmatic-hydrothermal stage and ended up in the mid hydrothermal stage.

4.3. Multi-element geochemistry

A summary of the multi-element geochemistry of the pegmatites in the Bewadze-Mankoadze area is presented in Table 1. The following are the average concentrations and ranges of concentration (minimum and maximum) for the most significant elements: 0.69 ppm and 0.30–0.95 ppm for MgO; 260 ppm and 10.5–773 ppm for Ta; 38.5 ppm and 3.80–74.1 ppm for Nb; 851 ppm and 30.4–3465 ppm for Rb; 178 ppm and 10.0–551 ppm for Cs; 625 ppm and 22.0–1326 ppm for Cr; 417 ppm and 1.00–1574 ppm for Sm; 35.1 ppm and 1.80–92.3 ppm for Sc; 42.3 ppm and 23.5–60.4 ppm for Ga. This shows that the pegmatites are enriched in Cr, Cs, Rb, Sm, and Ta and the rest having low concentrations as shown in the box and whisker plot (Fig. 6). Cs, Rb, and Ta have bulk continental crust abundances of 2.00 ppm, 49.0 ppm, and 0.70 ppm, respectively [39]. Compared to these crustal abundances, the Bewadze-Mankoadze pegmatites show remarkable enrichment in these elements as reported above, similar to the pegmatites of the

Table 1
Summary statistics of the multi-element geochemical data obtained (concentrations of the major elements are in wt% and that of the minor elements are in ppm).

Element	No.	Min.	Max.	Mean	STD	Skewness	Kurtosis
Na_2O	12	0.72	3.80	2.80	0.88	−1.28	1.75
MgO	12	0.30	0.95	0.69	0.16	−0.97	2.34
Al_2O_3	12	10.8	18.5	12.8	2.27	1.74	2.6
SiO_2	12	43.6	55.6	47.5	3.51	1.03	1.11
K_2O	12	0.13	3.89	1.70	1.54	0.43	−1.71
CaO	12	0.03	2.72	0.55	0.77	2.48	6.02
Fe_2O_3	12	0.16	31.2	3.38	8.79	3.43	11.8
V	12	10.0	94.0	62.4	26.0	−1.45	1.40
Cr	12	22.0	1326	625	405	0.05	−0.86
Co	12	4.50	17.0	9.13	4.26	0.88	−0.53
Ni	12	15.3	68.6	31.4	14.0	1.83	4.23
Cu	12	1.50	4.10	2.42	0.70	1.19	2.31
Zn	12	3.30	344	68.5	95.6	2.52	7.03
Ga	12	23.5	60.4	42.3	8.66	−0.19	2.63
As	12	0.40	12820	1836	4340	2.20	3.73
Rb	12	30.4	3465	851	1081	1.58	2.08
Y	12	0.50	3.00	1.30	0.82	0.83	−0.07
Zr	12	6.10	291	60.0	99.6	2.03	2.73
Nb	12	3.80	74.1	38.5	25.5	0.18	−1.29
Cs	12	10.0	551	178	145	1.50	3.34
Ba	12	13.0	501	104	155	2.00	3.43
La	12	17.0	20.0	18.8	0.87	−0.44	0.23
Ce	12	24.0	61.0	32.0	11.6	1.99	3.28
Hf	12	2.80	14.3	5.75	3.76	1.49	1.33
Pb	12	0.90	13.2	3.06	3.88	2.22	4.21
Th	12	0.60	2.50	1.32	0.71	0.40	−1.36
U	12	5.70	9.70	7.32	1.11	0.56	0.66
Ta	12	10.5	773	259	250	1.03	0.06
Sm	12	1.00	1574	417	573	1.08	−0.24
Sc	12	1.80	92.3	35.1	31.4	0.70	−0.92

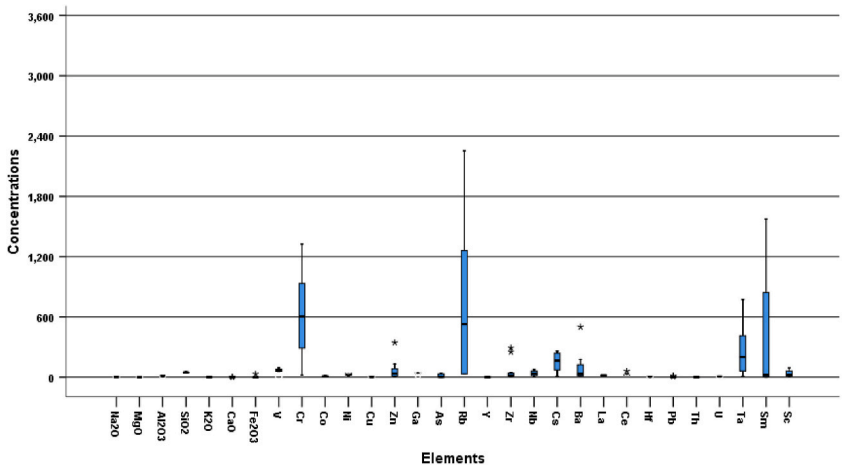

Fig. 6. Box and Whisker plot showing the elemental concentration from the geochemical analysis.

Cape Coast sedimentary Basin of the Birimian Supergroup of Ghana [32], the pegmatites of the Zenaga inlier in the Anti-Atlas, Morocco [33] and the Shigar Valley pegmatites, Pakistan [34]. The elevated concentrations of these elements especially, Cs and Rb in the pegmatites-aplites indicates the occurrence of pollucite in the area as reported by Ref. [1].

4.4. Implications of the petrographic analysis

The presence of quartz veinlets points to hydrothermal activities in the area. The columbite group of minerals, which formed during the waning phase of the magmatic stage contribute to the high tantalum content due to the existence of tantalite in them. Other minerals which contribute to the geochemistry in the area include albite, muscovite and tourmaline. They formed at the end of the magmatic stage transitioning into the magmatic-hydrothermal stage of the pegmatite emplacement and these minerals contributed to

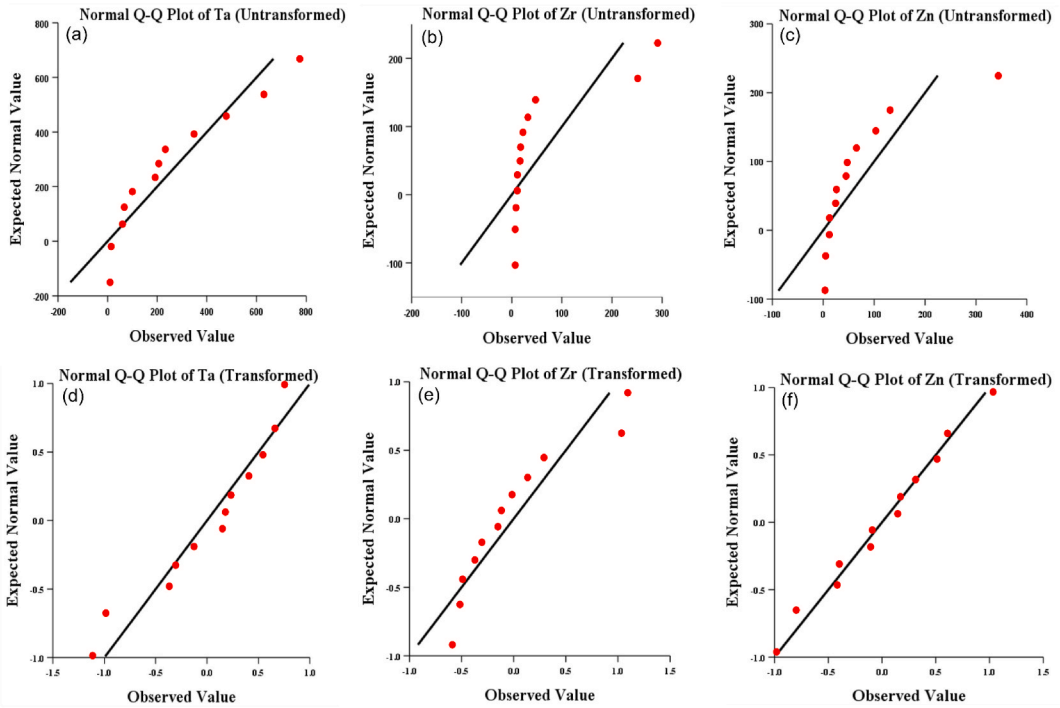

Fig. 7. Q-Q Plots of Tantalum (Ta), Zircon (Zr) and Zinc (Zn) distributions before and after centred log-ratio transformation.

Table 2
Kolmogorov-Smirnov and Shapiro-Wilk tests for normality using untransformed geochemical data (values highlighted in red are <0.05).

Tests of Normality						
Element	Kolmogorov-Smirnov[a]			Shapiro-Wilk		
	Statistic	df	Sig.	Statistic	df	Sig.
Na_2O	0.163	12	0.200*	0.904	12	0.177
MgO	0.152	12	0.200*	0.935	12	0.435
Al_2O_3	0.27	12	0.016	0.796	12	0.008
SiO_2	0.162	12	0.200*	0.91	12	0.211
K_2O	0.209	12	0.154	0.835	12	0.024
CaO	0.422	12	0.00	0.604	12	0.00
Fe_2O_3	0.478	12	0.00	0.393	12	0.00
V	0.266	12	0.019	0.793	12	0.008
Cr	0.105	12	0.200*	0.97	12	0.914
Co	0.244	12	0.047	0.859	12	0.048
Ni	0.244	12	0.047	0.827	12	0.019
Cu	0.202	12	0.189	0.909	12	0.205
Zn	0.264	12	0.02	0.679	12	0.001
Ga	0.215	12	0.133	0.917	12	0.265
As	0.494	12	0.00	0.489	12	0.00
Rb	0.224	12	0.099	0.79	12	0.007
Y	0.186	12	0.200*	0.893	12	0.13
Zr	0.389	12	0.00	0.576	12	0.00
Nb	0.145	12	0.200*	0.924	12	0.321
Cs	0.202	12	0.189	0.869	12	0.064
Ba	0.34	12	0.00	0.664	12	0.00
La	0.28	12	0.01	0.884	12	0.099
Ce	0.299	12	0.004	0.695	12	0.001
Hf	0.277	12	0.012	0.775	12	0.005
Pb	0.401	12	0.00	0.605	12	0.00
Th	0.223	12	0.10	0.871	12	0.067
U	0.133	12	0.200*	0.963	12	0.821
Ta	0.209	12	0.155	0.878	12	0.082
Sm	0.327	12	0.001	0.761	12	0.004
Sc	0.21	12	0.149	0.891	12	0.123

Table 3
Kolmogorov-Smirnov and Shapiro-Wilk tests for normality using transformed geochemical data (values highlighted in red are <0.05).

Tests of Normality						
Element	Kolmogorov-Smirnov[a]			Shapiro-Wilk		
	Statistic	df	Sig.	Statistic	df	Sig.
Na_2O	0.252	12	0.033	0.742	12	0.002
MgO	0.213	12	0.141	0.816	12	0.014
Al_2O_3	0.253	12	0.033	0.84	12	0.028
SiO_2	0.163	12	0.200*	0.924	12	0.317
K_2O	0.173	12	0.200*	0.873	12	0.071
CaO	0.253	12	0.033	0.909	12	0.204
Fe_2O_3	0.184	12	0.200*	0.876	12	0.079
V	0.387	12	0.00	0.629	12	0.00
Cr	0.245	12	0.045	0.824	12	0.018
Co	0.161	12	0.200*	0.921	12	0.292
Ni	0.184	12	0.200*	0.953	12	0.686
Cu	0.15	12	0.200*	0.965	12	0.858
Zn	0.099	12	0.200*	0.985	12	0.997
Ga	0.228	12	0.085	0.87	12	0.065
As	0.209	12	0.153	0.818	12	0.015
Rb	0.209	12	0.156	0.862	12	0.052
Y	0.165	12	0.200*	0.907	12	0.197
Zr	0.177	12	0.200*	0.857	12	0.044
Nb	0.187	12	0.200*	0.871	12	0.066
Cs	0.155	12	0.200*	0.912	12	0.227
Ba	0.222	12	0.107	0.848	12	0.035
La	0.286	12	0.007	0.88	12	0.089
Ce	0.237	12	0.061	0.77	12	0.004
Hf	0.244	12	0.047	0.865	12	0.056
Pb	0.235	12	0.066	0.802	12	0.01
Th	0.217	12	0.124	0.849	12	0.036
U	0.126	12	0.200*	0.976	12	0.962
Ta	0.18	12	0.200*	0.925	12	0.327
Sm	0.261	12	0.024	0.819	12	0.016
Sc	0.139	12	0.200*	0.921	12	0.293

the geochemistry of the pegmatites in the area as Rb, Cr and Sm were dominant. These elements form part of the chemistry of the minerals that were dominant from the petrographic studies.

4.5. Multivariate statistical analysis

The multivariate statistical analysis considered every element whose concentration was measured as part of the geochemical data.

4.5.1. Q-Q plots

Q-Q plots of Ta, Zr and Zn in Fig. 7a–c, showed a deviation from the normal line. As geochemical data hardly follows normal distribution, it indicates that the raw dataset is the result of several associations of elements, which might be connected to various geochemical processes [40]. Extreme sample concentrations that seemed to be separate from the others were also noticed. Outliers are seen in samples where certain element concentrations do not match the normal distribution [23]. Outliers in geochemistry are likely indications of abnormalities connected to mineralization. As was already mentioned, these outliers are also typical of other geochemical processes.

Centred log-ratio transformation was used to rectify them. By minimising the difference between the highest and lowest values in the dataset, this transformation normalises the data and lessens the impact of outliers. Q-Q plots of the transformed data were shown in Fig. 7d–f and compared with the untransformed Q-Q plots.

4.5.2. Kolmogorov-Smirnov and Shapiro Wilk tests

After the data was converted using the centred log-ratio transformation to test for normality, the Kolmogorov-Smirnov Test and Shapiro Wilk Test were carried out on the raw dataset. The test results indicate clearly that a few elements from the raw dataset had a p-value greater than 0.05 in both the Kolmogorov-Smirnov and Shapiro Wilk tests (Table 2). Most of the p-values were greater than 0.05 after the data was subjected to centred log ratio transformation (Table 3).

4.5.3. Correlation analysis

Spearman correlation was used to assess the degree of correlation between the elements of interest. Since Spearman is a nonparametric measure of rank correlation and may be used to assess a monotonic connection between variables, it was preferred to alternatives like Pearson and Kendall. The Spearman correlation (Table 4) found a significant positive correlation between Ta and Cu

Table 4
Spearman correlation analysis ($r \geq 0.50$).

	Na_2O	MgO	Al_2O_3	SiO_2	K_2O	CaO	Fe_2O_3	V	Cr	Co	Ni	Cu	Zn	Ga	As	Rb	Y	Zr	Nb	Cs	Ba	La	Ce	Hf	Pb	Th	U	Ta	Sm	Sc
Na_2O	1.00																													
MgO	−0.16	1.00																												
Al_2O_3	−0.70	−0.41	1.00																											
SiO_2	−0.32	0.46	0.22	1.00																										
K_2O	−0.73	−0.02	**0.79**	**0.52**	1.00																									
CaO	0.07	−0.70	0.22	−0.70	−0.32	1.00																								
Fe_2O_3	−0.22	0.07	0.01	0.07	−0.15	0.19	1.00																							
V	0.07	0.48	−0.21	**0.63**	0.23	−0.82	−0.21	1.00																						
Cr	−0.13	−0.07	0.08	0.16	−0.06	0.10	0.00	−0.33	1.00																					
Co	−0.30	−0.24	0.26	−0.13	−0.14	**0.53**	**0.77**	−0.39	0.22	1.00																				
Ni	−0.51	−0.14	**0.64**	**0.54**	**0.56**	−0.09	0.41	0.15	−0.22	0.31	1.00																			
Cu	−0.56	0.21	0.17	0.17	0.28	0.06	0.28	−0.28	**0.59**	0.32	−0.12	1.00																		
Zn	−0.04	**0.55**	−0.45	0.17	−0.17	−0.32	0.40	0.33	−0.06	0.31	−0.15	0.35	1.00																	
Ga	−0.04	0.16	−0.18	−0.15	−0.11	0.05	0.00	−0.11	0.27	0.28	−0.39	0.43	**0.70**	1.00																
As	−0.06	0.00	0.08	−0.18	−0.23	0.22	**0.60**	−0.24	−0.17	0.50	0.27	−0.24	−0.09	−0.32	1.00															
Rb	−0.75	0.29	**0.52**	0.46	**0.85**	−0.46	−0.04	0.24	−0.05	−0.10	0.36	0.45	0.24	0.25	−0.34	1.00														
Y	−0.80	0.05	**0.77**	**0.52**	**0.97**	−0.29	−0.01	0.15	−0.01	−0.05	**0.57**	0.41	−0.09	−0.08	−0.23	**0.90**	1.00													
Zr	−0.22	0.12	0.30	0.06	−0.11	0.19	0.32	−0.30	0.23	0.45	0.27	−0.08	−0.22	−0.15	**0.70**	−0.18	−0.08	1.00												
Nb	0.15	**0.72**	−0.70	0.11	−0.43	−0.26	−0.02	0.20	0.11	−0.15	−0.49	0.32	**0.61**	0.40	−0.32	−0.08	−0.35	−0.18	1.00											
Cs	−0.45	0.42	0.22	0.25	**0.52**	−0.35	−0.10	−0.12	0.08	−0.31	0.01	0.48	0.13	0.27	−0.24	**0.73**	**0.60**	−0.06	0.14	1.00										
Ba	−0.27	−0.48	**0.54**	−0.25	0.25	0.28	−0.02	−0.27	0.26	0.29	0.05	0.03	−0.45	−0.18	0.44	−0.01	0.18	0.35	−0.71	−0.18	1.00									
La	−0.39	−0.47	0.49	−0.25	0.17	**0.58**	**0.63**	−0.38	−0.08	**0.78**	0.38	0.25	0.01	−0.05	**0.51**	0.01	0.20	0.18	−0.48	−0.25	**0.52**	1.00								
Ce	0.23	−0.69	0.19	−0.55	−0.20	**0.74**	0.12	−0.48	0.00	0.40	−0.13	−0.08	−0.30	−0.07	0.39	−0.50	−0.28	0.08	−0.45	−0.45	**0.55**	**0.67**	1.00							
Hf	−0.63	−0.18	**0.67**	0.13	0.40	0.28	0.38	−0.40	0.50	**0.64**	0.32	**0.54**	−0.06	0.15	0.41	0.27	0.43	**0.54**	−0.38	0.17	**0.66**	**0.64**	0.37	1.00						
Pb	−0.47	−0.38	**0.80**	0.40	**0.78**	0.00	0.01	0.06	−0.10	−0.04	**0.70**	0.02	−0.56	−0.59	0.05	0.38	**0.73**	0.01	−0.68	0.11	0.38	0.39	0.18	0.38	1.00					
Th	−0.77	−0.30	**0.87**	0.37	**0.80**	0.11	0.12	−0.22	0.25	0.19	**0.64**	0.44	−0.39	−0.27	−0.04	**0.56**	**0.83**	0.11	−0.51	0.33	0.38	0.43	0.05	**0.64**	**0.85**	1.00				
U	−0.44	−0.19	0.31	−0.29	0.06	**0.50**	0.44	−0.50	0.34	**0.78**	−0.05	**0.60**	0.34	**0.56**	0.29	0.14	0.11	0.24	−0.08	0.05	0.45	**0.72**	0.48	**0.77**	−0.09	0.25	1.00			
Ta	−0.03	0.37	−0.33	0.16	0.00	−0.23	−0.13	0.05	0.41	−0.11	−0.46	**0.65**	**0.62**	**0.76**	−0.62	0.32	0.06	−0.45	**0.66**	0.48	−0.45	−0.33	−0.31	−0.04	−0.44	−0.14	0.23	1.00		
Sm	−0.62	0.48	0.11	0.29	0.22	−0.33	**0.50**	0.18	0.08	0.28	0.27	0.36	0.21	−0.23	0.45	0.31	0.31	0.32	0.08	0.11	0.25	0.29	−0.29	0.38	0.13	0.28	0.23	−0.16	1.00	
Sc	−0.01	0.40	−0.38	0.10	−0.06	−0.18	−0.07	0.03	0.40	−0.05	−0.52	**0.69**	**0.66**	**0.76**	−0.57	0.27	0.01	−0.43	**0.70**	0.43	−0.42	−0.27	−0.25	−0.03	−0.48	−0.19	0.29	**0.99**	−0.11	1.00

Table 5
Rotated component matrix showing the distribution of elements into factors.

Rotated Component Matrix[a]							
Component							
Element	1	2	3	4	5	6	7
Pb	−0.898	−0.059	**0.378**	−0.103	0.035	0.037	0.098
Ce	−0.885	0.209	−0.125	−0.025	−0.069	−0.137	**0.286**
Ga	**0.843**	−0.262	0.243	0.088	−0.136	−0.266	0.185
Nb	**0.832**	−0.239	−0.263	0.269	0.065	0.207	−0.132
MgO	**0.822**	−0.290	0.103	−0.224	−0.098	0.391	−0.088
Sc	**0.787**	−0.328	−0.020	0.434	−0.070	0.083	0.235
Ta	**0.785**	−0.380	−0.016	0.459	−0.081	−0.011	0.099
Zn	**0.764**	−0.222	−0.149	−0.026	0.408	0.095	0.376
Cs	**0.677**	−0.078	0.559	−0.040	−0.237	−0.075	−0.188
Zr	−0.214	**0.922**	−0.043	0.091	0.180	0.089	−0.025
As	−0.314	**0.880**	−0.095	−0.076	0.228	0.067	0.194
V	**0.360**	−0.860	−0.060	−0.200	0.013	0.123	−0.176
Hf	−0.279	**0.674**	0.352	0.488	0.058	0.116	0.270
Ba	−0.541	**0.650**	0.102	−0.122	−0.323	0.143	0.316
CaO	−0.426	**0.627**	−0.183	−0.004	0.123	−0.546	0.221
Co	−0.074	**0.604**	−0.074	0.134	0.579	−0.072	0.455
Y	0.058	−0.043	**0.970**	0.023	0.105	0.164	0.075
K_2O	−0.100	−0.079	**0.943**	−0.178	0.080	0.230	0.034
Rb	0.203	−0.121	**0.930**	−0.078	0.112	0.183	0.009
Th	−0.417	0.187	**0.780**	0.336	0.066	0.084	0.039
Al_2O_3	−0.167	0.323	**0.768**	0.221	−0.005	−0.396	0.207
Cr	0.269	0.298	−0.166	**0.854**	−0.118	−0.015	−0.071
Cu	0.294	0.037	0.255	**0.783**	−0.011	0.379	0.287
Ni	−0.157	0.108	0.441	−0.179	**0.783**	0.081	−0.173
Fe_2O_3	0.087	0.181	0.014	−0.033	**0.760**	0.087	0.265
Sm	0.027	0.450	0.174	0.028	0.414	**0.719**	0.192
Na_2O	−0.141	−0.186	−0.540	−0.340	**0.190**	−0.676	−0.049
SiO_2	−0.023	−0.285	0.408	0.320	0.330	**0.633**	−0.209
U	0.179	0.529	0.126	0.223	0.080	0.023	**0.771**
La	−0.351	0.383	0.191	0.007	0.330	−0.061	**0.754**

Table 6
Total variance explained for transformed dataset.

Total Variance Explained						
Factor	Initial Eigenvalues			Extraction Sums of Squared Loadings		
	Total	**% of Variance**	**Cumulative %**	**Total**	**% of Variance**	**Cumulative %**
1	10.467	34.891	34.891	10.467	34.891	34.891
2	6.542	21.807	56.698	6.542	21.807	56.698
3	4.607	15.358	72.056	4.607	15.358	72.056
4	2.554	8.513	80.569	2.554	8.513	80.569
5	2.053	6.843	87.412	2.053	6.843	87.412
6	1.309	4.363	91.776	1.309	4.363	91.776
7	1.074	3.579	95.355	1.074	3.579	95.355

(r = 0.65), Ta and Zn (r = 0.62), Ta and Nb (r = 0.66), Sc and Cu (r = 0.69), Sc and Zn (r = 0.66) as well as Sc and Ga (r = 0.76).

A high to strong positive correlation between the constituent components indicates their paragenetic existence [41]. The distribution of the elements in the region was caused by intricate geochemical processes [23]. Thus, similar mechanisms are responsible for their enrichment. The negative correlation between some elements is caused by a variety of processes, including the distribution and concentration of elements caused by deformational activity during metamorphic events and hydrothermal enhancement or deposition of elements. The element of interest, Ta correlates moderately to strongly with Sc, Ga, Nb, and Cs. This may be an indication that Sc, Ga, Nb, and Cs could have occurred paragenetically with Ta.

4.5.4. Factor analysis (FA)

Seven (7) factors, which defined 95.355 % of the total variance having eigenvalues more than 1 were extracted in the FA (Table 5). Factor 1 accounts for 34.891 % of the total variance (Table 6) and is composed of Ta-Cs-Zn-Nb-MgO-Sc-Ga-V multi-element association (Fig. 8). This factor's elements are generated by wall rock and host rocks. Ta-Nb-MgO-Sc-Ga-V are usually associated with the host rocks and that of Cs-Zn are associated with the wall rocks [42]. Factor 2 explains 21.807 % of the total variance (Table 6) and is composed of Hf-Zr-Ba-CaO-As-Co multi-element association (Fig. 8). This factor is mainly associated with host rocks and arsenic (As) in

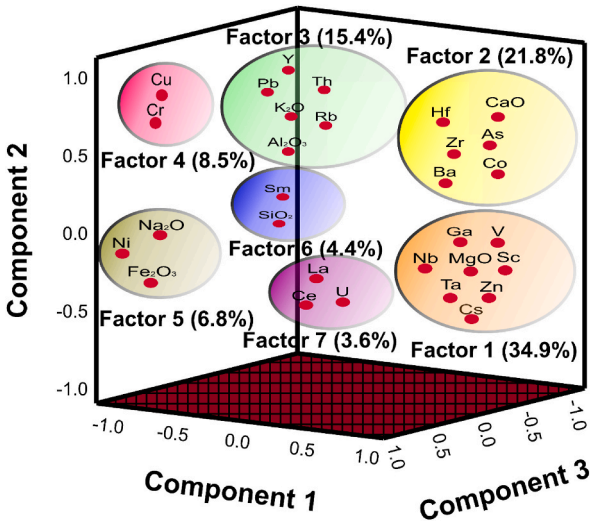

Fig. 8. Rotated component matrix showing the factors and total variances in percentages.

this factor may be derived from hydrothermal sources.

Factor 3 also accounts for 15.358 % of the total variance (Table 6) and is made up of Y-Pb-K_2O-Al_2O_3-Th-Rb association (Fig. 8), which are mainly from the wall rocks with Pb from hydrothermal sources. Factor 4 makes up 8.513 % of the total variance (Table 6) and is composed of Cr-Cu mainly sourced from mafic lithologies and hydrothermal fluids. Factor 5 with Na_2O-Fe_2O_3-Ni element association (Fig. 8) explains 6.843 % of the total variance (Table 6), which is associated with a mixture of the wall rocks and the host rocks.

Factor 6 explains 4.363 % of the total variance (Table 6) and is made up of SiO_2-Sm association (Fig. 8) and is associated with wall rocks of the pegmatites, which are the gneisses from the Birimian Supergroup. Factor 7 with La-Ce-U association (Fig. 8) accounts for 3.579 % of the total variance of the data (Table 6). La-Ce is of the host rocks and U is from the hydrothermal sources [43].

4.5.5. *Hierarchical cluster analysis for transformed dataset*

The dendrogram generated from the transformed dataset shows three groups of multi-element relationships (Fig. 9). Cluster 1 has multi-element associations of Zr, As, La, Hf, CaO, U, Co, Pb, Ce, Ba and Na_2O; cluster 2 consists of V, Nb, Ta, Ga, Sc, Cr, Cu, Nb and MgO multi-element association; and cluster 3 is made up of multi-element association of Ni, SiO_2, Cs, Zn, Sm, Rb, K_2O, Y, Th, Al_2O_3 and Fe_2O_3 (Fig. 9). This confirms the sources inferred from the FA, mainly from the host rocks, wall rocks, and hydrothermal sources.

4.5.6. *Comparison of multivariate statistical techniques*

Using the dataset from the centred log-ratio, cluster 2 with element associations of Ta-V-Nb-Ga-Sc-Cr-Cu-MgO and factor 1 with element association of Ta-Cs-Zn-Nb-MgO-Sc-Ga-V from factor analysis show similar elemental association of Ta-Nb-Ga-Sc. Cesium (Cs) was also considered due to its similarity with tantalum and was also found to correlate good with Ta and in the same factor with Ta as well. Considering all these, using cluster 2 from the HCA, factor 1 from the FA, and also the correlation analysis, Sc-Ga-Nb-Cs could be considered as the elemental cluster associated with tantalum deposits in the Bewadze-Mankoadze area.

4.6. *Single and multi-element halo mapping*

4.6.1. *Mapping single element geochemical anomalies*

Single element halo maps were plotted for the elements as shown in Figs. 10 and 11a-d. Green to light green colouration indicates low elemental concentrations, yellowish green to yellow indicates moderate elemental concentrations while the orange to red shows high anomalous concentrations of the elements. The Ta anomaly map (Fig. 10) showed notable Ta anomalous concentration in the south-western part of the study with moderate concentrations towards the northeastern part of the study area.

Anomaly maps for Sc, Ga, Nb and Cs are shown in Fig. 11a–d. Scandium (Sc) anomaly of the study shows high concentrations in the south-western domain of the study area and reduced toward the north-eastern part of the study area. Gallium (Ga) geochemical anomaly showed high concentrations in the middle of the southwestern domain of the study area. Niobium (Nb) anomaly map also shows high concentrations in the southwestern side of the study area. Cs showed high concentrations in the southwestern and a few moderate to high concentration in the northern part of the study area. These patterns clearly overlap with the pattern displayed by Ta (Fig. 10). Hence, they can indeed be regarded as pathfinder elements of Ta.

4.6.2. *Multi-element anomaly mapping and exploration implications*

Using the thresholds as computed and geochemical halos, characterised by the presence of high concentration of pathfinder

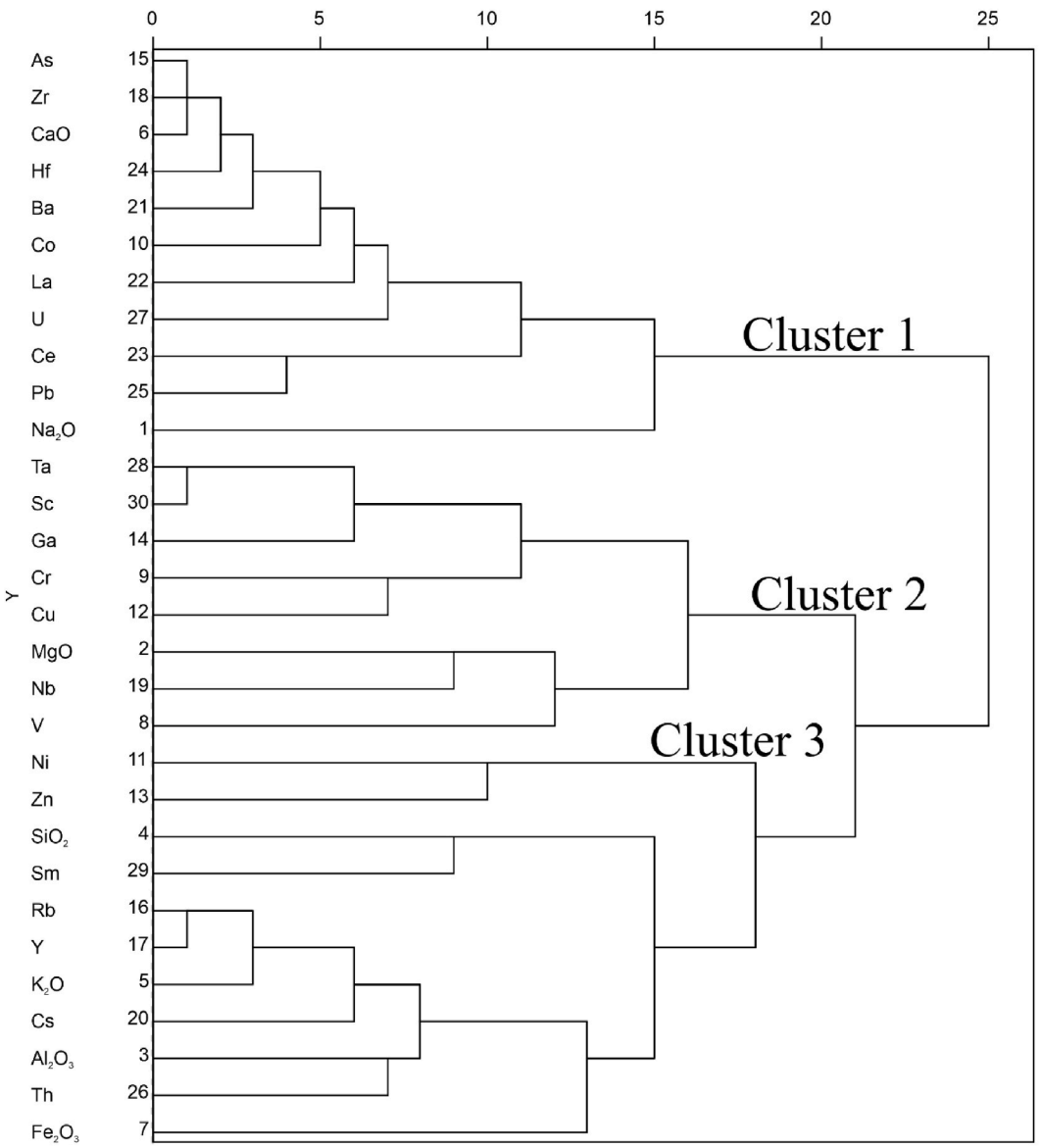

Fig. 9. Dendrogram from hierarchical cluster analysis showing three (3) elemental clusters.

elements in relation to Ta mineralization, multi-element halo maps were generated. These multi-elemental anomaly maps were produced based on the elemental relationships. The Ta-Sc, Ta-Ga, Ta-Nb (Fig. 12a–c) maps show moderate to high concentrations in the south-western part of the study area and low concentrations towards the north-eastern part of the study area. The Ta-Cs anomaly map (Fig. 12d) shows high concentrations in the southwestern corridor of the study area and moderate concentrations in the north-eastern part of the study area. Ta-Sc-Ga-Nb-Cs (Fig. 13) map shows moderate to very high concentrations in the southwestern corridor and low to very low concentrations towards the northeastern corridor.

From this study, the multi-element patterns reveal similar geochemical anomalies that are concentrated in the south-western part of the study area. Prospecting for tantalum should therefore focus on this area and the pegmatites serve as host rocks of the tantalum in the Bewadze-Mankoadze area. This suggests that using these elements as pathfinder elements can significantly enhance tantalum mineral discovery in the area.

4.7. Implications and guide to tantalum exploration

Tantalum is only found in significant amounts in granitic pegmatites that belong to the rare-element category of orogenic pegmatite associations [44]. These pegmatites are abundant in southern Ghana, especially in Ewoyaa, Biriwa, Winneba, Bewadze, and

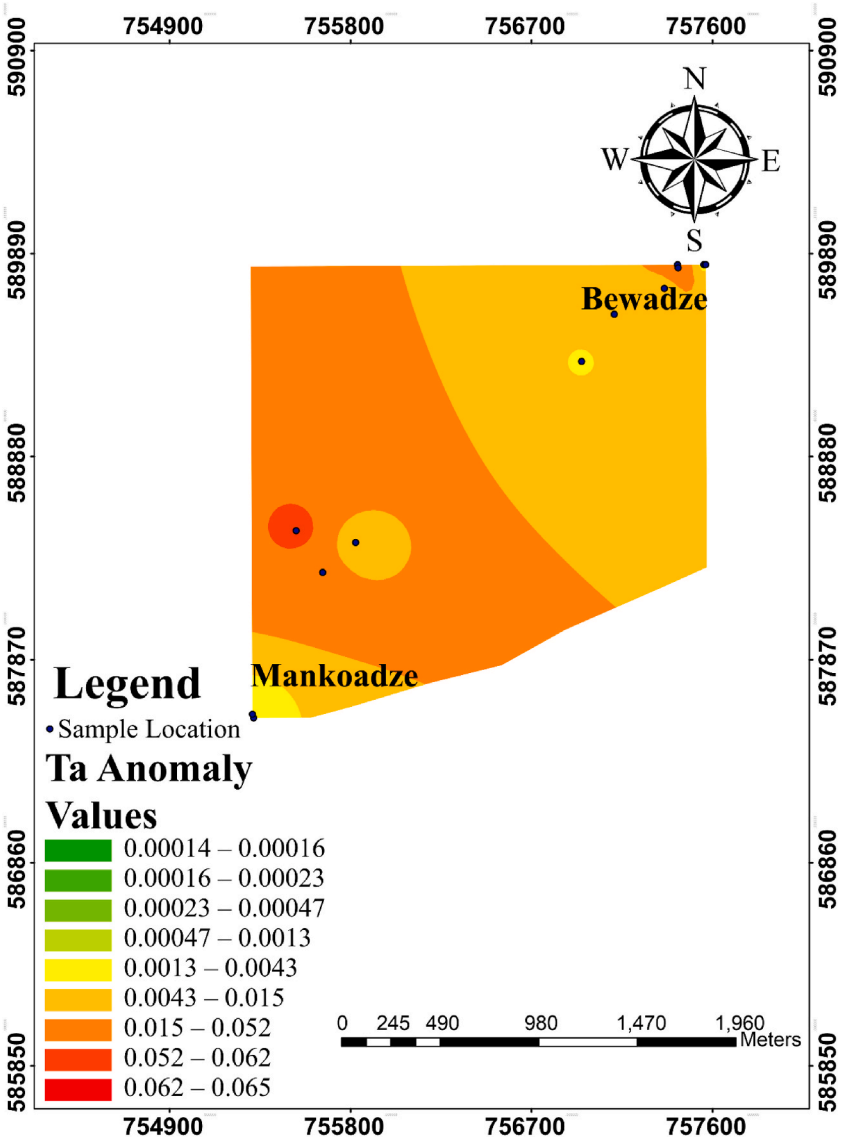

Fig. 10. Single element halo maps showing the anomaly distribution of Ta.

Mankoadze areas. In the Bewadze-Mankoadze pegmatite field, post-tectonic intrusions of productive granites and their pegmatite aureoles are connected to fault systems or lithologic boundaries within schists and gneisses containing quartz, K-feldspar, plagioclase, albite, muscovite, spodumene, tourmaline, columbite group minerals, and montebrasite as confirmed by the petrographic analysis in this study. Specific granite and pegmatite clusters might have tantalum mineralization in the pegmatitic-granite domes of the original granites, typically located in pegmatites at the outer edges of the aureoles. Decreasing metamorphic grade in host rocks, increasing complexity in texture and paragenesis of pegmatites, evolving typomorphic minerals, and higher fractionation [7] suggest areas with greater tantalum potential.

The geochemical data reveals that the pegmatites are enriched in Cr, Cs, Rb, Sm, and Ta. These elements are reported in literature as pathfinders to LCT pegmatites [9–11], hence confirming that the Ta pegmatites in this study are indeed LCT-type pegmatites. Multivariate statistics identified Sc, Ga, Nb, and Cs as the primary elements associated with Ta in the Bewadze-Mankoadze area. Geochemical anomalies related to these elements are present in the southern part of the study area, as indicated by single and multi-element halo mapping. Exploration for Ta mineralization should concentrate on the southern-western region of the study area, where anomalies of the pathfinder elements are situated. To evaluate the overall level of fractionation for Ta enrichment, different geochemical indicators are present in individual pegmatitic granites and pegmatite bodies in the study area. In the initial phase of exploration for Ta-pegmatites in the Bewadze-Mankoadze area, the relationship between Ta and Cs in coarse-grained early white mica is found to be the most informative indicator. Albitization of pegmatites commonly conceals the original zonal pattern yet enhances the recoverable quantity of Ta oxides [45]. Hence, albitized pegmatites undergoing metasomatic changes with high levels of both Ta and

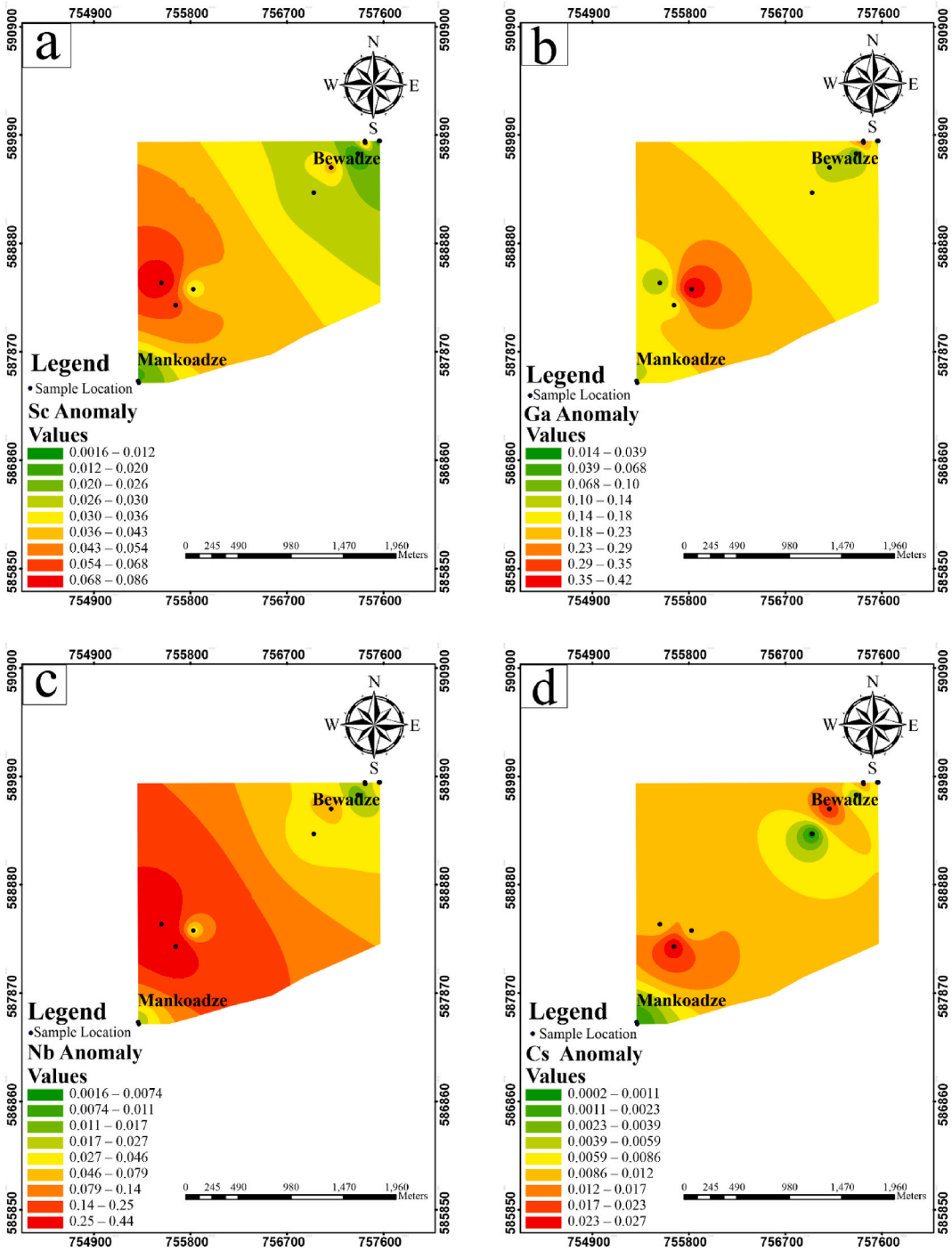

Fig. 11. Single element halo maps showing the anomaly distribution of (a) Sc (b) Ga (c) Nb and (d) Cs.

Cs are the most promising targets for exploration. Geochemical and geophysical techniques can be used to locate and delineate the Ta-pegmatite deposits.

5. Conclusion

This study focused on hard rock geochemistry of the Bewadze-Mankoadze area. Petrographic studies reveal the presence of plagioclase, quartz, spodumene, columbite group minerals, albite, tourmaline, muscovite, potassium feldspar and montebrasite. Cr, Cs,

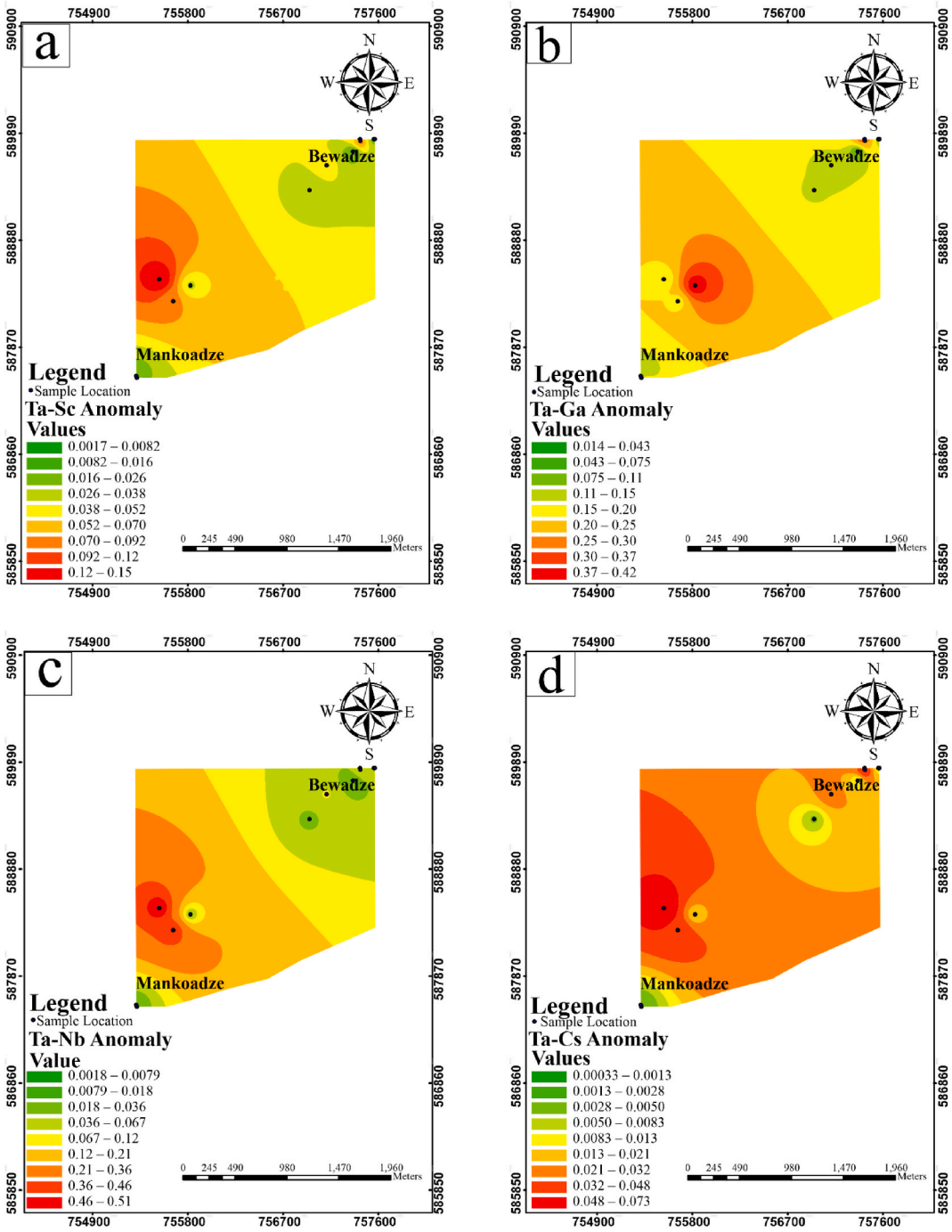

Fig. 12. Multi-element halo maps showing the anomaly distribution of (a) Ta-Sc (b)Ta-Ga (c) Ta-Nb (d) Ta-Cs.

Rb, Sm, and Ta are the most dominating elements in the Bewadze-Mankoadze area, according to box and whisker plots. Q-Q plots involving the untransformed geochemical data showed sporadic behaviour revealing that different geological processes contributed to the mineralization in the area. Spearman's Correlation, factor analysis and hierarchical cluster analysis indicated Sc, Ga, Nb and Cs as pathfinders of Ta and can be associated directly to the pegmatites in the Bewadze-Mankoadze area. Geochemical anomaly maps reveal high anomaly values of Ta and its identified pathfinder elements in the south-western corridor. Hence, exploration activities for Ta mineralization should focus on the south-western corridor, where the anomalies of the pathfinder elements are located. During the preliminary investigation of Ta-pegmatites in the Bewadze-Mankoadze area, the correlation between Ta and Cs in coarse-grained early white mica proves to be the most significant marker. The original zonal pattern in pegmatites is often obscured by albitization, but it

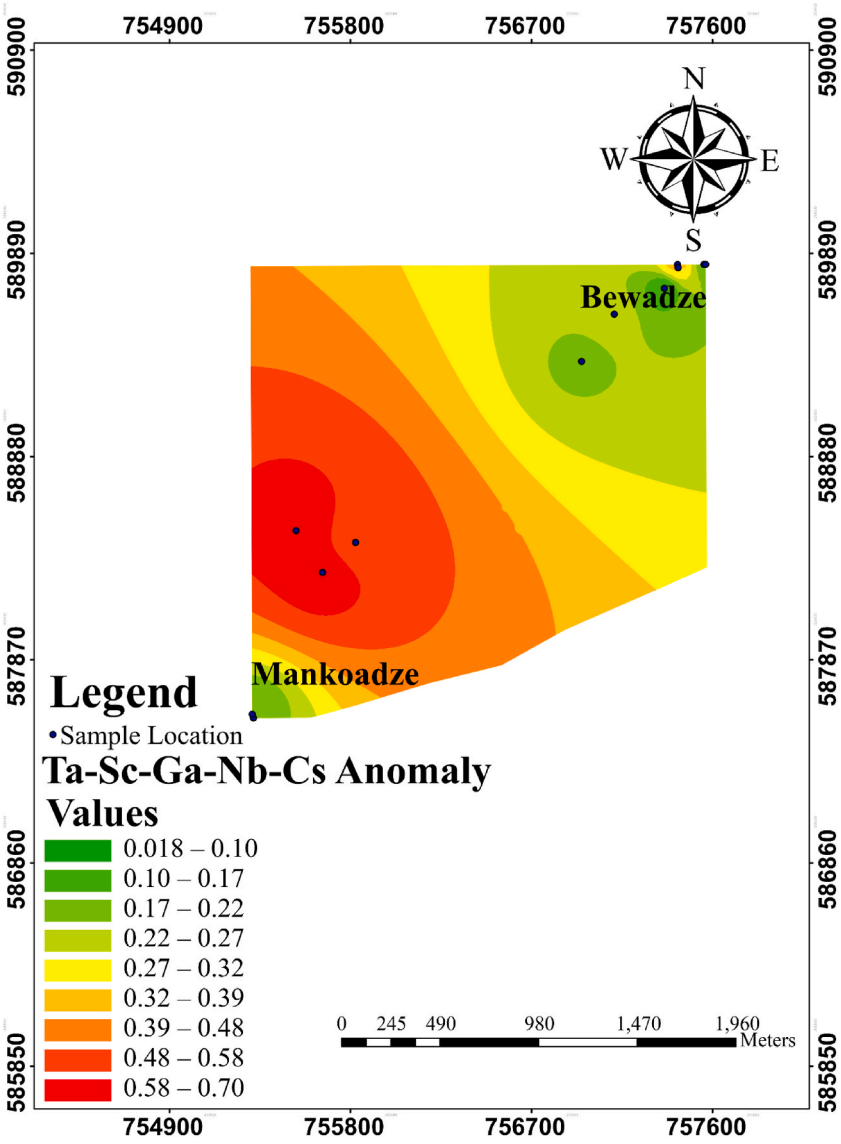

Fig. 13. Multi-element halo maps showing the anomaly distribution of Ta-Sc-Ga-Nb-Cs.

increases the amount of recoverable Ta oxides. Therefore, pegmatites that have been altered by albitization and are experiencing metasomatic changes with significant concentrations of both Ta and Cs present the most potential for exploration.

This study is a contribution to the global transition to clean energy since Ta is a critical mineral that can be used in the production of capacitors. Tantalum capacitors play a crucial role in energy-saving technologies, such as renewable energy systems. They facilitate effective storage and transportation of energy in solar panels, wind turbines, and electric vehicles, aiding in decreasing reliance on fossil fuels and decreasing greenhouse gas emissions. Therefore, if the Ta deposit is economically harnessed, it will boost the foreign exchange earnings of Ghana, and the by-products can be used for clean energy production in the country. Moreover, the Ta-bearing pegmatites in the Bewadze-Mankoadze area contain a wide variety of precious minerals, including spodumene, beryl, and tourmaline. These minerals frequently appear as massive, properly formed crystals, and their presence raises the market value of pegmatites in Ghana. In all, the discovery of the Ta-bearing pegmatites in the Bewadze-Mankoadze area adds to the list of granitic rare-element pegmatites and rare-metal granites found in Africa. This study did not investigate the age of the Ta-bearing pegmatites and the timing of the ore settlement as well as the fluid evolution history. Therefore, it is recommended that detailed geochronological, stable isotopes, and fluid inclusion studies be carried out on the Ta-bearing pegmatites in the area to constrain the age of the pegmatites and the mineralization and the genesis of the Ta ore.

Data and code availability statement

Data included in article.

CRediT authorship contribution statement

Emmanuel Daanoba Sunkari: Writing – review & editing, Writing – original draft, Visualization, Validation, Supervision, Software, Resources, Project administration, Methodology, Investigation, Funding acquisition, Formal analysis, Data curation, Conceptualization. **Joshua Nkansah:** Writing – review & editing, Writing – original draft, Visualization, Validation, Software, Methodology, Investigation, Formal analysis, Data curation, Conceptualization. **Salaam Jansbaka Adams:** Writing – review & editing, Writing – original draft, Visualization, Validation, Supervision, Resources, Project administration, Methodology, Funding acquisition.

Declaration of competing interest

The authors declare that they have no known competing financial interests or personal relationships that could have appeared to influence the work reported in this paper.

Acknowledgement

This research is part of the second author's BSc project work under the supervision of the first author at the University of Mines and Technology, Ghana. The Government of Ghana is duly appreciated for the financial support through the Book and Research Allowance to Faculty Members.

References

[1] A.K. Agomor, Geological indications and prospecting guide to rare metalmineralisation of birimian granite pegmatite of Ghana, in: Proceeding of the International Conference on the Geology of Ghana with Emphasis on Gold, vol. 1, Geological Survey Department, Accra, Ghana, 1987, pp. 2–24.
[2] P. Černý, Rare-element granitic pegmatites Part I: anatomy and internal evolution of pegmatite deposits, Geosci. Can. 18 (2) (1991) 49–67. https://id.erudit.org/iderudit/geocan18_2art01.
[3] C.I. Chalokwu, M.A. Ghazi, E.E. Foord, Geochemical characteristics and K Ar ages of rare-metal bearing pegmatites from the Birimian of southeastern Ghana, J. Afr. Earth Sci. 24 (1–2) (1997) 1–9, https://doi.org/10.1016/S0899-5362(97)00022-5.
[4] R.L. Linnen, M. Van Lichtervelde, P. Černý, Granitic pegmatites as sources of strategic metals, Elements 8 (4) (2012) 275–280, https://doi.org/10.2113/gselements.8.4.275.
[5] S.J. Adams, Rare-metal mineralization of the winneba-mankoadze pegmatites, southwestern Ghana; MPhil thesis. Graduate School of Nuclear and Allied Sciences, University of Ghana, 2013, pp. 1–101pp.
[6] S.J. Adams, M. Van Lichtervelde, P.O. Amponsah, P.M. Nude, D.K. Asiedu, S.B. Dampare, Characterisation and rare-metal potential of the Winneba-Mankoadze pegmatites, Southern Ghana: evidence of two pegmatite fields, J. Afr. Earth Sci. 207 (2023) 105049, https://doi.org/10.1016/j.jafrearsci.2023.105049.
[7] S.J. Adams, E.D. Sunkari, J.E.K. Hanson, K.K. Tandoh, S.E.K. Tetteh, P.M. Nude, D.K. Asiedu, S.B. Dampare, Geochemistry of the Winneba-Mankoadze pegmatites in southern Ghana: a clue to the petrogenesis of the pegmatites, Ore and Energy Resource Geology 17 (2024) 100051, https://doi.org/10.1016/j.oreoa.2024.100051.
[8] D. London, Ore-forming processes within granitic pegmatites, Ore Geol. Rev. 101 (2018) 349–383, https://doi.org/10.1016/j.oregeorev.2018.04.020.
[9] P. Černý, T.S. Ercit, The classification of granitic pegmatites revisited, Can. Mineral. 43 (6) (2005) 2005–2026.
[10] H.G. Dill, Pegmatites and aplites: their genetic and applied ore geology, Ore Geol. Rev. 69 (2015) 417–561, https://doi.org/10.1016/j.oregeorev.2015.02.022.
[11] H.G. Dill, The CMS classification scheme (chemical composition – mineral assemblage – structural geology) – linking geology to mineralogy of pegmatitic and aplitic rocks, Neues Jahrbuch Mineral. Abhand. 193 (3) (2016) 231–263, https://doi.org/10.1127/njma/2016/0304.
[12] A. Guastoni, LCT (lithium, cesium, tantalum) and NYF (niobium, yttrium, fluorine) pegmatites in the central alps. Proxies of exhumation history of the alpine nappe stack in the lepontine dome. PhD Thesis in Earth Science. Italy, University of Padua, 2012, p. 161.
[13] B. Bekele, A.K. Sen, The mineral chemistry of gahnite, garnet and columbite-group minerals (CGM): implications for genesis and evolution of the Kenticha Rare-element granite-pegmatite, Adola, Ethiopia, J. Afr. Earth Sci. 162 (2020) 103691, https://doi.org/10.1016/j.jafrearsci.2019.103691.
[14] T.S. Ercit, L.A. Groat, R.A. Gault, Granitic pegmatites of the O'Grady batholith, NWT, Canada: a case study of the evolution of the elbaite subtype of rare-element granitic pegmatite, Can. Mineral. 41 (1) (2003) 117–137.
[15] S.L. Lee, M. Doxbeck, J. Mueller, M. Cipollo, P. Cote, Texture, structure and phase transformation in sputter beta tantalum coating, Surf. Coating. Technol. 177–178 (2004) 44–51, https://doi.org/10.1016/j.surfcoat.2003.06.008.
[16] F. Melcher, T. Graupner, T. Oberthür, P. Schütte, Tantalum-(niobium-tin) mineralisation in pegmatites and rare-metal granites of Africa, S. Afr. J. Geol. 120 (1) (2017) 77–100, https://doi.org/10.25131/gssajg.120.1.77.
[17] J. Agyei-Duodu, G.K. Loh, K.O. Boamah, M. Baba, W. Hirdes, M. Toloczyki, D.W. Davis, Geological Survey Department of Ghana (GSD), Geological Map of Ghana, Accra, Ghana, 2009, pp. 1–1000000. Report.
[18] K.K. Tandoh, S.F. Gbedemah, M.R.S. Doku, S.J. Adams, B.A. Brako, Petrographic and structural analysis of Paleoproterozoic Birimian granitoids and associated rocks of Boankra areas in the Kumasi Basin of Ghana, Arabian J. Geosci. 16 (1) (2023) 8, https://doi.org/10.1007/s12517-022-11010-8.
[19] B. Eisenlohr, The Structural Geology of Birimian and Tarkwaian Rocks of Southwest Ghana: Republic of Ghana. Federal Republic of Germany, Technical Cooperation Project No. 80.2040. 6, BGR, 1989.
[20] B.N. Eisenlohr, W. Hirdes, The structural development of the early proterozoic birimian and tarkwaian rocks of southwest Ghana, west Africa, J. Afr. Earth Sci. 14 (3) (1992) 313–325, https://doi.org/10.1016/0899-5362(92)90035-B.
[21] R.J. Griffis, K. Barning, F.L. Agezo, F.K. Akosah, Gold deposits of Ghana, Minerals Commission Report (2002) 19–37.
[22] E.D. Sunkari, M. Appiah-Twum, A. Lermi, Using laterite geochemistry for exploration of orogenic gold deposits in the Wa-Lawra belt, NW Ghana: kunche in perspective. Ömer Halisdemir Üniversitesi Mühendislik Bilimleri Dergisi, Niğde Ömer Halisdemir Üniversitesi 7 (3) (2018) 1137–1141, https://doi.org/10.28948/ngumuh.502334.
[23] E.D. Sunkari, M. Appiah-Twum, A. Lermi, Spatial distribution and trace element geochemistry of laterites in Kunche area: implication for gold exploration targets in NW, Ghana, J. Afr. Earth Sci. 158 (2019) 103519, https://doi.org/10.1016/j.jafrearsci.2019.103519.
[24] R.R. Wilcox, Understanding and Applying Basic Statistical Methods Using R, John Wiley & Sons, 2016, p. 478.
[25] M.A. Stephens, EDF statistics for goodness of fit and some comparisons, J. Am. Stat. Assoc. 69 (347) (1974) 730–737, https://doi.org/10.1080/01621459.1974.10480196.

[26] W.J. Conover, Practical Nonparametric Statistics, third ed., John Wiley & Sons, Inc., New York, 1999, pp. 428–433.
[27] C. Spearman, The proof and measurement of association between two things, Am. J. Psychol. 100 (3/4) (1987) 441–471, https://doi.org/10.2307/1422689.
[28] J. Zhao, S. Chen, R. Zuo, Identifying geochemical anomalies associated with Au–Cu mineralization using multifractal and artificial neural network models in the Ningqiang district, Shaanxi, China, J. Geochem. Explor. 164 (2016) 54–64, https://doi.org/10.1016/j.gexplo.2015.06.018.
[29] P.M. Nude, J.M. Asigri, S.M. Yidana, E. Arhin, G. Foli, J.M. Kutu, Identifying pathfinder elements for gold in multi-element soil geochemical data from the Wa-Lawra belt, Northwest Ghana: a multivariate statistical approach, Int. J. Geosci. 3 (1) (2012) 62–70, https://doi.org/10.4236/ijg.2012.31008.
[30] F.N. David, J.W. Tukey, Exploratory data analysis, Biometrics 33 (4) (1977), https://doi.org/10.2307/2529486, 768-768.
[31] A.P. Reis, A.J. Sousa, E. Cardoso Fonseca, Soil geochemical prospecting for gold at marrancos (northern portugual), J. Geochem. Explor. 73 (1) (2001) 1–10, https://doi.org/10.1016/S0375-6742(01)00169-8.
[32] P.M. Nude, J.E.K. Hanson, S.B. Dampare, T.T. Akiti, S. Osae, E.S. Nyarko, N. Zkaria, S. Enti-Brown, Geochemistry of Pegmatites associated with the cape coast granite complex in the Egyaa and Akim Oda areas of southern Ghana, Ghana J. Sci. 51 (2011) 89–100. https://www.ajol.info/index.php/gjs/article/view/116697.
[33] Y. Morsli, Y. Zerhouni, A. Wafik, A. Elouazzani, S. Alikouss, A. Saidi, Z. Baroudi, Eburneen pegmatites of the Zenaga inlier (Anti-Atlas, Morocco): petrography, geochemistry, and classification, J. Afr. Earth Sci. 186 (2022) 104438, https://doi.org/10.1016/j.jafrearsci.2021.104438.
[34] M. Hassan, Mineralogy and Geochemistry of the Gemstones and the Gemstone- Bearing Pegmatites in the Shigar Valley of Skardu Northern Areas of Pakistan, PhD Thesis, National Centre of Excellence in Geology, University of Peshawar, 2007, pp. 1–361.
[35] E.D. Sunkari, B.M. Kore, S.E.K. Tetteh, Petrography and structural features of the Precambrian basement rocks in the Benin-Nigerian Shield, NW Nigeria: implications for their correlation with South Atlantic Precambrian terranes, AIMS Geosciences 8 (4) (2022) 503–524, https://doi.org/10.3934/geosci.2022028.
[36] T. Roy, B. Plante, M. Benzaazoua, I. Demers, Geochemistry and mineralogy of a spodumene-pegmatite lithium ore at various mineral beneficiation stages, Miner. Eng. 202 (2023) 108312, https://doi.org/10.1016/j.mineng.2023.108312.
[37] P. Černý, The Tanco rare-element pegmatite deposit, Manitoba; regional context, internal anatomy, and global comparisons, in: R.L. Linnen, I.M. Samson (Eds.), Rare Element Geochemistry and Mineral Deposits, vol. 17, Geological Association of Canada Short Course Notes, 2005, pp. 127–158.
[38] M. Van Lichtervelde, S. Salvi, D. Beziat, R.L. Linnen, Textural features and chemical evolution in tantalum oxides: magmatic versus hydrothermal origins for Ta mineralization in the Tanco Lower pegmatite, Manitoba, Canada, Econ. Geol. 102 (2) (2007) 257–276, https://doi.org/10.2113/gsecongeo.102.2.257.
[39] R.L. Rudnick, Composition of the continental crust. The Crust, Treatise on Geochemistry 3 (2005) 17–18.
[40] R. Zuo, Identifying geochemical anomalies associated with Cu and Pb–Zn skarn mineralization using principal component analysis and spectrum–area fractal modeling in the Gangdese Belt, Tibet (China), J. Geochem. Explor. 111 (1–2) (2011) 13–22, https://doi.org/10.1016/j.gexplo.2011.06.012.
[41] D.J. Lapworth, K.V. Knights, R.M. Key, C.C. Johnson, E. Ayoade, M.A. Adekanmi, T.M. Arisekola, O.A. Okunlola, B. Backman, M. Eklund, P.A. Everett, R. T. Lister, J. Ridgway, M.J. Watts, S.J. Kemp, P.E.J. Pitfield, Geochemical mapping using stream sediments in west-central Nigeria: implications for environmental studies and mineral exploration in West Africa, Appl. Geochem. 27 (6) (2012) 1035–1052, https://doi.org/10.1016/j.apgeochem.2012.02.023.
[42] R. Morgenstern, R.E. Turnbull, M.P. Hill, P.M.J. Durance, M.S. Rattenbury, Rare earth element mineral potential in New Zealand, GNS sci consult Rep 23 (2018) 243–250.
[43] S. Makvandi, G. Beaudoin, M.B. Beth McClenaghan, D. Quirt, P. Ledru, PCA of Fe-oxides MLA data as an advanced tool in provenance discrimination and indicator mineral exploration: case study from bedrock and till from the Kiggavik U deposits area (Nunavut, Canada), J. Geochem. Explor. 197 (2019) 199–211, https://doi.org/10.1016/j.gexplo.2018.11.013.
[44] P. Černý, Exploration strategy and methods for pegmatite Depositsof tantalum, in: P. Moller, P. Černý, F. Saupe, Tantalum Lanthanides, Niobium (Eds.), Special Publication No. 7 of the Society for Geology Applied to Mineral Deposits, Springer, Berlin, 1989, pp. 274–302, https://doi.org/10.1007/978-3-642-87262-4_13.
[45] P. Möller, G. Morteani, Geochemical exploration guide for tantalum pegmatites, Econ. Geol. 82 (7) (1987) 1888–1897, https://doi.org/10.2113/gsecongeo.82.7.1888.